THE JOURNAL OF BIOLOGICAL CHEMISTRY
Vol. 279, No. 46, Issue of November 12, pp. 48292–48306, 2004

Printed in U.S.A.

Structural Analysis of the Complement Control Protein (CCP) Modules of $GABA_B$ Receptor 1a

ONLY ONE OF THE TWO CCP MODULES IS COMPACTLY FOLDED*[S]

Received for publication, June 11, 2004, and in revised form, July 30, 2004
Published, JBC Papers in Press, August 9, 2004, DOI 10.1074/jbc.M406540200

Stanislas Blein‡§, Rachel Ginham¶‖, Dušan Uhrin‡, Brian O. Smith‡, Dinesh C. Soares‡, Stefvan Veltel‡, R. A. Jeffrey McIlhinney¶, Julia H. White‡‡, and Paul N. Barlow‡§§**

From the ‡Edinburgh Protein Interaction Centre, University of Edinburgh, West Mains Road, Edinburgh EH9 3JJ, Scotland, United Kingdom, the ¶Anatomical Neuropharmacology Unit, Medical Research Council, Mansfield Road, Oxford OX1 3TH, United Kingdom, and ‡‡Pathway Discovery, Genomics and Proteomic Sciences, GlaxoSmithKline Medicines Research Centre, Gunnels Wood Road, Stevenage SG1 2NY, United Kingdom

The γ-aminobutyric acid type B ($GABA_B$) receptor is a heterodimeric G-protein-coupled receptor. In humans, three splice variants of the $GABA_B$ receptor 1 (R1) subunit differ in having one, both, or neither of two putative complement control protein (CCP) modules at the extracellular N terminus, prior to the GABA-binding domain. The *in vivo* function of these predicted modules remains to be discovered, but a likely association with extracellular matrix proteins is intriguing. The portion of the $GABA_B$ R1a variant encompassing both of its CCP module-like sequences has been expressed, as have the sequences corresponding to each individual module. Each putative CCP module exhibits the expected pattern of disulfide formation. However, the second module (CCP2) is more compactly folded than the first, and the three-dimensional structure of this more C-terminal module (expressed alone) was solved on the basis of NMR-derived nuclear Overhauser effects. This revealed a strong similarity to previously determined CCP module structures in the regulators of complement activation. The N-terminal module (CCP1) displayed conformational heterogeneity under a wide range of conditions whether expressed alone or together with CCP2. Several lines of evidence indicated the presence of native disorder in CCP1, despite the fact that recombinant CCP1 contributes to binding to the extracellular matrix protein fibulin-2. Thus, we have shown that the two CCP modules of $GABA_B$ R1a have strikingly different structural properties, reflecting their different functions.

γ-Aminobutyric acid (GABA)[1] is the principal inhibitory neurotransmitter of the vertebrate central nervous system. It is the ligand for both ionotropic GABA type A receptors and metabotropic GABA type B ($GABA_B$) receptors. $GABA_B$ receptors belong to G-protein-coupled receptor class III, which includes metabotropic glutamate receptors, Ca^{2+}-sensing receptors, and some pheromone and taste receptors (1). Agonist and antagonists of $GABA_B$ receptors have been shown to be effective in clinical cases or animal models of nociception, depression, addiction, epilepsy, and cognitive impairment. Selective $GABA_B$ receptor ligands could also be useful in the treatment of peripheral nervous system disorders (2, 3).

The $GABA_B$ receptor is composed of subunits termed $GABA_B$ R1 and $GABA_B$ R2, both of which are needed for receptor function (4–7). The two subunits share a similar molecular architecture, common to all class III G-protein-coupled receptors, consisting of a large extracellular N-terminal domain encompassing a ligand-binding site, followed by a transmembrane heptahelical domain and an intracellular C-terminal tail. Coupling to G-proteins is mediated by the intracellular loops connecting the transmembrane helices and the C-terminal region.

In class III G-protein-coupled receptors, the extracellular domain of each subunit is proposed to have a dynamic bilobate structure, where the two globular lobes form a "clamshell"-like shape. The current model for the function of these dimers suggests that upon ligand binding, closure of the two lobes in only one of the two domains is sufficient to create a relative change in orientation between the two subunits, which in turn results in the activation of G-proteins (8). In the case of $GABA_B$ receptors, this model is consistent with the observations that only the $GABA_B$ R1 subunit is able to bind $GABA_B$ agonists or antagonists with measurable potency (5, 6), that the $GABA_B$ R2 subunit is important for coupling to G-proteins (9, 10), and

* The costs of publication of this article were defrayed in part by the payment of page charges. This article must therefore be hereby marked "*advertisement*" in accordance with 18 U.S.C. Section 1734 solely to indicate this fact.

[S] The on-line version of this article (available at http://www.jbc.org) contains "Supplemental Results."

The atomic coordinates and structure factors (codes 1SRZ and 1SS2) have been deposited in the Protein Data Bank, Research Collaboratory for Structural Bioinformatics, Rutgers University, New Brunswick, NJ (http://www.rcsb.org/).

The list of ^1H, ^{15}N, and ^{13}C resonance assignments of $GABA_B$ R1a CCP2 has been submitted to BioMagResBank with accession numbers BMRB 6171 and BMRB 6166.

§ Supported by an industrial partnership grant from the United Kingdom Biotechnology and Biological Sciences Research Council and GlaxoSmithKline.

‖ Recipient of a GlaxoSmithKline Ph.D. studentship.

** Present address: Div. of Biochemistry and Molecular Biology, Inst. of Biomedical and Life Sciences, Joseph Black Bldg., University of Glasgow, Glasgow G12 8QQ, Scotland, UK.

§§ To whom correspondence should be addressed: Edinburgh Protein Interaction Centre, Joseph Black Chemistry Bldg., University of Edinburgh, West Mains Rd., Edinburgh EH9 3JJ, Scotland, UK. Tel.: 44-131-650-4727; Fax: 44-131-650-7055; E-mail: Paul.Barlow@ed.ac.uk.

[1] The abbreviations used are: GABA, γ-aminobutyric acid; $GABA_B$, γ-aminobutyric acid type B; $GABA_B$ R, γ-aminobutyric acid type B receptor; CCP, complement control protein; CCP1, first complement control protein module of $GABA_B$ R1a (Gly^{17}–Ile^{98}); CCP2, second complement control protein module of $GABA_B$ R1a (Val^{96}–Asn^{159}); CCP12, complement control protein module pair of $GABA_B$ R1a (Gly^{17}–Asn^{159}); DAF, decay-accelerating factor; BMG, buffered minimal glycerol; YNB, yeast nitrogen base; DTT, dithiothreitol; Ab, antibody; F2C, fibulin-2 C-terminal residues 1069–1184; GST, glutathione *S*-transferase; HA, hemagglutinin; CHO, Chinese hamster ovary; Trx, thioredoxin; GdnHCl, guanidine hydrochloride; DSC, differential scanning calorimetry; ANS, 1-anilinonaphthalene-8-sulfonic acid; HSQC, heteronuclear single quantum coherence; TOCSY, total correlation spectroscopy; NOESY, nuclear Overhauser effect spectroscopy; NOE, nuclear Overhauser effect; r.m.s.d., root mean square deviation.

that the heptahelical region of the $GABA_B$ R1 subunit also influences coupling efficacy (11). Further evidence that the $GABA_B$ R1 and $GABA_B$ R2 subunit extracellular domains are in direct contact is provided by time-resolved fluorescence resonance energy transfer experiments (12).

With regard to the $GABA_B$ R1 subunit, three splice variants are defined by the presence of one (human $GABA_B$ R1c), two (human/rat $GABA_B$ R1a), or neither (human/rat $GABA_B$ R1b) of the putative complement control protein (CCP) modules at the N terminus, prior to the GABA-binding domain (13, 14). Two other variations of the $GABA_B$ R1 subunit occur: in the fifth extracellular loop (rat $GABA_B$ R1c) and at the C terminus (human $GABA_B$ R1d) (13, 15). Finally, $GABA_B$ R1e is a soluble truncated version of $GABA_B$ R1a (16). The human $GABA_B$ R1c splice variant is unrelated to rat $GABA_B$ R1c and differs from $GABA_B$ R1a in that it has a 62-amino acids deletion that removes the second CCP module-like sequence. The function of $GABA_B$ R1c has not been reported, but reverse transcription-PCR studies showed up-regulation of this variant in fetal brain (13). Thus, it is the presence of the putative N-terminal CCP modules that is the differentiating factor between three of the principal variants discovered so far. Significant differences in expression levels within tissues and during development occur between $GABA_B$ heterodimers containing $GABA_B$ R1a *versus* those containing $GABA_B$ R1b (13). There are, however, no known differences in the pharmacological profiles of the two (17). In this respect, observations that the putative CCP modules of $GABA_B$ R1a interact with the extracellular matrix are intriguing (17–21).

The 143 residues distinguishing $GABA_B$ R1a from $GABA_B$ R1b are thought to form a tandemly arranged pair of CCP modules (22, 23), the only examples of CCP modules suspected to occur in any seven-transmembrane domain receptor. CCP modules are the predominant module type within several soluble and cell-surface regulators of complement activation (24), but another example of a central nervous system protein that contains CCP modules is the 87.6-kDa human equivalent to mouse SEZ-6 (25, 26). SEZ-6 is a single transmembrane domain mouse protein of unknown function whose expression is enhanced by perfusion of brain slices with convulsant drugs. Although some examples of CCP modules act merely as structural or spacer units in bigger proteins, wherever they occur toward the N terminus of a well studied cell-surface protein, they have been shown to participate in specific protein-protein interactions (22).

The three-dimensional structure of a typical CCP module has a compact hydrophobic core containing conserved residues sandwiched between small antiparallel β-sheets. Four conserved cysteines are disulfide-linked Cys-I–Cys-III and Cys-II–Cys-IV. The sequence of the first putative CCP module of $GABA_B$ R1a (CCP1) is a less typical example of a CCP module than the second CCP module-like sequence (CCP2) and has an insertion of 12 residues (Arg^{43}–Asn^{54}; numbering refers to the rat $GABA_B$ R1a amino acid sequence and includes the signal sequence) that would be expected to be part of the "hypervariable" loop (22). There is also an N-terminal extension of seven residues (Gly^{17}–Asn^{23}) in CCP1 that is not part of the CCP module consensus. *N*-Glycosylation sites found in the $GABA_B$ R1a CCPs are exclusively located in the CCP1 amino acid sequence (at Asn^{23} and Asn^{83}).

We now show that the two CCP modules of $GABA_B$ R1a have striking structural differences. The first module is not compactly folded, whereas CCP2 is a regular CCP module with particularly high structural similarity to the third module of the decay-accelerating factor (DAF) of complement. Despite being poorly structured, CCP1 exhibits the standard disulfide pattern and is able, like the intact $GABA_B$ R1a subunit, to bind the extracellular matrix protein fibulin-2.

EXPERIMENTAL PROCEDURES

Construction of Expression Vectors encoding CCP1, CCP2, and CCP12—DNA fragments encoding rat CCP1 (Gly^{17}–Ile^{98}), CCP2 (Val^{96}–Asn^{159}), and CCP12 (Gly^{17}–Asn^{159}) were amplified by PCR using a DNA template prepared by Dr. Edward Hawrot (Brown University, Providence, RI). The sense primer used to amplify the CCP1 and CCP12 DNA fragments was designed to include the first seven residues of the mature rat $GABA_B$ R1a gene product so that the first residue of the recombinant protein corresponds to Gly^{17}, which immediately follows the putative signal peptide sequence. The sense primer for the CCP2 DNA fragment was designed to include the three "linker" residues (Val^{96}–Ile^{98}) between the fourth consensus Cys of CCP1 and the first consensus Cys of CCP2. The antisense primer used to amplify the CCP2 and CCP12 DNA fragments was designed to include the three residues following the fourth consensus Cys of CCP2; the antisense primer used to amplify CCP1 was designed to include Val^{96}–Ile^{98}. All sense primers incorporated an EcoRI restriction site, and all antisense primers incorporated a NotI restriction site as well as two stop codons. Each resulting PCR product was gel-purified, digested with EcoRI/NotI, and ligated into the same sites of the pPICZαA yeast expression vector (Invitrogen, Paisley, UK). All plasmids were sequenced to confirm the desired DNA sequence and the correct reading frame. DNA midi-preparations of the expression constructs were prepared using the Wizard Plus midi-preparation DNA purification kit (Promega, Southampton, UK). For each CCP construct, 10 μg of SacI-linearized plasmid were electroporated into *Pichia pastoris* strain KM71H(Mut^S) according to the recommendations of Invitrogen. Zeocin-resistant colonies were then tested for protein expression; colonies expressing the most recombinant protein were picked for large-scale protein preparations.

Expression and Isotope Labeling—For each protein construct, a single colony was used to inoculate a starter culture (10 ml) of buffered minimal glycerol (BMG; 100 mM potassium phosphate (pH 6 or 3), 1.34% (w/v) yeast nitrogen base (YNB; with $(NH_4)_2SO_4$ and without amino acids), 1% (v/v) glycerol, and 0.00004% (w/v) biotin). After 2 days of incubation at 30 °C (250 rpm), this starter culture was diluted to 1 liter with BMG; equal portions were transferred into four 1-liter baffled flasks; and the flasks were shaken at 30 °C for an additional 2 days ($A_{600\ nm} \sim 13$–15). Cells were then pelleted at 1500 $\times$ *g* for 5 min at room temperature and transferred to 200 ml of buffered minimal methanol medium (100 mM potassium phosphate (pH 6 or 3), 1.34% (w/v) YNB (with $(NH_4)_2SO_4$ and without amino acids), 0.5% (v/v) methanol, and 0.00004% (w/v) biotin) for induction. Inductions were performed over 5 days at 25 °C. Cells were resuspended in fresh induction medium daily, and supernatants were stored at −20 °C with protease inhibitors (1 mM phenylmethanesulfonyl fluoride and 5 mM EDTA) while awaiting purification.

For ^{15}N isotope labeling, cultures were grown in modified BMG in which 1.34% (w/v) YNB was replaced with 0.34% (w/v) YNB (without $(NH_4)_2SO_4$ and without amino acids) supplemented with 0.2% (w/v) $(^{15}NH_4)_2SO_4$ (^{15}N/YNB). For $^{13}C/^{15}N$ isotope labeling, a $^{13}C/^{15}N$ buffered minimal dextrose medium (100 mM potassium phosphate (pH 6 or 3), ^{15}N/YNB, 0.5% (w/v) [^{13}C]glucose, and 0.00004% (w/v) biotin) was used instead of BMG. Cells were then harvested by centrifugation as described above and resuspended in 100 mM potassium phosphate (pH 3), ^{15}N/YNB, 0.1% (w/v) [^{13}C]glycerol, and 0.00004% (w/v) biotin for 2 h prior to induction. This stage allows a smooth transition between glucose and methanol as the sole carbon source for the cells and was found to reduce cell death. Induction for both ^{15}N and $^{13}C/^{15}N$ isotope labeling was carried out using buffered minimal methanol medium containing ^{15}N/YNB instead of ^{14}N/YNB. For $^{13}C/^{15}N$ isotope labeling, buffered minimal methanol medium was prepared with [^{13}C]methanol. All isotopically labeled compounds were purchased from Cambridge Isotope Ltd. (Cambridge, MA).

Purification—Supernatants were filtered through a 0.2-μm filter and concentrated 50-fold using a combination of a preparative scale spiral wound filter module (Millipore, Watford, UK) linked to a peristaltic pump and an N_2-pressurized stirred cell (Millipore) at 4 °C. The concentrated proteins were purified by cation exchange chromatography (Mono S HR 5/5, Amersham Biosciences, Little Chalfont, UK) with a 0–1 M NaCl gradient over 25 column volumes; CCP1 and CCP12 were buffered in 12.5 mM sodium acetate (pH 5.3), and CCP2 was buffered in 50 mM sodium acetate (pH 4.6). Following this initial cation exchange step, CCP1 and CCP12 were deglycosylated with endoglycosidase H_f (3000 units/mg of recombinant protein) for 6–8 h at 37 °C. Endoglyco-

sidase H_f was removed by reloading the cleavage mixture onto the Mono S column; traces of glycosylated material were removed by concanavalin A-Sepharose chromatography (Amersham Biosciences). All recombinant fragments were further purified by reverse-phase chromatography (RP2 column, Applied Biosystems, Warrington, UK) with a 10–60% acetonitrile and 0.1% (v/v) trifluoroacetic acid gradient over 34 column volumes. Protein yields were on the order of 8 mg/preparation. The N-terminal sequence of each protein construct was confirmed by amino acid sequencing (Dr. A. Cronshaw, University of Edinburgh, Edinburgh, UK). Protein concentrations were calculated using absorbance at 280 nm and a theoretical extinction coefficient based on the protein sequence (ProtParam Tool, available at www.expasy.org).

Mass Spectrometry—All $GABA_B$ R1a CCP fragments were examined by mass spectrometry using positive electrospray ionization on a Micromass Platform-II instrument. The number of disulfide bonds present in CCP1 and CCP12 was deduced from a series of alkylation/reduction experiments using dithiothreitol (DTT) and neutralized iodoacetic acid treatment (27), followed by a combination of reverse-phase chromatography and electrospray ionization mass spectrometry. The disulfide bond pattern in a "truncated" version of CCP1 (lacking the seven-residue N-terminal extension) was analyzed by trypsin digestion and sequencing of the resulting fragments on a Micromass hybrid quadrupole time-of-flight mass spectrometer.

Binding Experiments—For antibody (Ab) production, a fragment of fibulin-2 containing the C-terminal residues 1069–1184 (F2C) was amplified using the appropriate primers. The product was cloned into the EcoRI/XhoI sites of the vector pGEX-4T-2 (Amersham Biosciences), and the protein was expressed in *Escherichia coli* strain BL21(DE3) pLysS. The resulting fusion protein, GST-F2C, was purified by affinity chromatography on glutathione-Sepharose and subsequently used to immunize New Zealand White rabbits. To produce an Ab specific to F2C, the rabbit serum was first absorbed onto Sepharose coupled to GST before purification with Sepharose coupled to GST-F2C. Both affinity resins were produced by coupling GST and GST-F2C to CNBr-activated Sepharose 4B (Sigma, Gillingham, UK) according to the manufacturer's recommendations.

To generate a stable cell line expressing fibulin, a DNA fragment encoding full-length fibulin-2 tagged with the hemagglutinin (HA) epitope at the N terminus was cloned in the pcIn6 vector (28) and transfected into Chinese hamster ovary (CHO) cells. Clones secreting the protein were primarily selected using 1 mg/ml Geneticin (Sigma). A stable cell line was subsequently produced by the limiting dilution method and maintained with 0.5 mg/ml Geneticin. The secreted fibulin could be detected in the cell medium as an immunoreactive band at ~200 kDa with the anti-F2C Ab or as a pair of bands at ~200 and 180 kDa using an anti-HA epitope monoclonal Ab (Santa Cruz Biotechnology, Santa Cruz, CA) (see Fig. 2*a*). The 180-kDa band probably represents a C-terminal cleavage of the protein, whereas the larger band is consistent with full-length fibulin-2 (29).

For production of larger quantities of an F2C-Sepharose resin, a DNA construct encoding the F2C domain was inserted in the pET-32a(+) vector using the NcoI and XhoI sites (Merck Biosciences, Nottingham, UK). The resulting plasmid allowed expression of the F2C domain as a fusion protein with thioredoxin (Trx) and various affinity purification tags between the two domains, including a polyhistidine tag (Trx-F2C). BL21(DE3) pLysS cells transformed with the Trx-F2C vector were grown to large-scale in LB selective broth (37 °C), and protein expression was induced by the addition of 1 mM isopropyl-β-D-thiogalactopyranoside for 3 h at 37 °C. Protein purification was performed using the Talon metal affinity resin (Clontech), and the purified protein was subsequently coupled to CNBr-activated Sepharose 4B. Similarly, we produced CCP12-, CCP1-, and CCP2-Sepharose by coupling purified CCP fragments (see above) to CNBr-activated Sepharose 4B.

Native $GABA_B$ receptors were prepared from rat brain synaptic membranes by sucrose gradient centrifugation using 6–8-week-old Sprague-Dawley rats (30). Solubilization of the membranes was achieved by incubating them at a detergent/protein ratio of 5:1 in 1% (w/v) sodium deoxycholate in 50 mM Tris-HCl (pH 8) containing protease inhibitors (Complete protease inhibitor mixture, Roche Diagnostics, Lewes, UK), 20 mM iodoacetamide, and 0.1 M NaCl for 15 min on ice. The lysate was adjusted to 0.2% (w/v) sodium deoxycholate with 50 mM Tris-HCl (pH 8) containing 1% (v/v) Triton X-100 and centrifuged at 67,000 × *g* for 1 h at 4 °C before aliquots were used in pull-down experiments with Trx-F2C-Sepharose.

Recombinant $GABA_B$ receptors were prepared from cells permanently expressing $GABA_B$ R1a or $GABA_B$ R1b with $GABA_B$ R2 subunits as described previously (31). Cells were grown to confluence in 25-cm^2 flasks, harvested, and then lysed in 1 ml of lysis buffer (50 mM Tris-HCl (pH 7.4), 1% (v/v) Triton X-100, 0.1 M NaCl, 1 mM $CaCl_2$, and 10 mM iodoacetamide supplemented with protease inhibitors (Complete protease inhibitor mixture)) for 15 min at 4 °C. The lysate was centrifuged at 14,000 rpm for 15 min at 4 °C, and aliquots of the supernatant were used in pull-down experiments with Trx-F2C-Sepharose.

Pull-down experiments were performed overnight at 4 °C using 100-μl volumes of the appropriate affinity supports and GST-Sepharose as a control resin. The beads were washed three times with lysis buffer and once with 50 mM Tris-HCl (pH 7.5) before the adsorbed proteins were eluted with SDS-PAGE sample loading buffer (62.5 mM Tris-HCl (pH 6.8), containing 1% (w/v) SDS, 5% (v/v) β-mercaptoethanol or 20 mM DTT, 0.005% (w/v) bromphenol blue, and 10% (v/v) glycerol) for 15 min at 60 °C. Eluted proteins were analyzed on either 7.5 or 6% SDS-polyacrylamide gels and immunoblotted with an anti-sheep $GABA_B$ R1 subunit Ab (4, 31) or the anti-HA epitope monoclonal Ab. Immunoblots were developed using the Supersignal substrate (Perbio Science, Tattenhall, UK) on a Bio-Rad Fluor-Smax imaging system.

Circular Dichroism Spectroscopy—Measurements were performed on a Jasco Model 810 spectropolarimeter. Measurements were recorded at 20 °C in 20 mM sodium phosphate (pH 7.5). The protein concentrations used were 12 and 36 μM in far- and near-UV experiments, respectively. Each CD spectrum represents the average of five scans (far-UV) or seven scans (near-UV) and was corrected by subtraction of a spectrum obtained for a solution lacking the protein but otherwise identical. The resulting spectrum was further smoothed using the Means-Movement method included in the Spectra-Manager software (Jasco Ltd., Great Dunmow, UK).

Plots of percentage fraction unfolded *versus* concentration of guanidine hydrochloride (GdnHCl) were derived from the average of five points, the maximal ellipticity and readings at ±1.2 and ±2.4 nm, to smooth experimental errors in the curves. Measurements were performed in triplicate, and pH was verified to be 7.5 in all GdnHCl-containing samples. The concentrations of GdnHCl stock solutions were confirmed using an Abbé Model B refractometer (Zeiss, Oberkochen, Germany) and applying the formula $[M] = 57.147(\Delta N) + 38.68(\Delta N)^2 - 91.6(\Delta N)^3$, where ΔN is the difference between the refraction coefficient of the buffer and that of the GdnHCl solution (made with the same buffer) being assayed (32).

Reduction of the disulfide bonds was performed by adding DTT to a final concentration of 10–20 mM to the different protein fragments using a 1.25 M stock solution. Samples were then left to equilibrate overnight at 20 °C under N_2.

Differential Scanning Calorimetry (DSC)—Calorimetric measurements were carried out on a VP-DSC differential scanning microcalorimeter (MicroCal, Northampton, UK) at the Microcalorimetry Facility of the University of Glasgow by Prof. Alan Cooper. The cell volume was 0.5 ml; the heating rate was 1 °C/min; and the excess pressure was kept at 25 p.s.i. All protein fragments were used at a concentration of 40 μM in 20 mM sodium phosphate (pH 7.5). The molar heat capacity of each protein was estimated by comparison with duplicate samples containing identical buffer from which the protein had been omitted. The partial molar heat capacities and melting curves were analyzed using standard procedures (33).

1-Anilinonaphthalene-8-sulfonic Acid (ANS) Fluorescence Measurements—Fluorescence emission spectra were recorded with a Fluoromax-3 spectrometer (Jobin-Yvon Ltd., Middlesex, UK). Protein samples (3.6 μM) in 20 mM sodium phosphate (pH 7.5) were mixed with 20 μM ANS (Molecular Probes Europe, Leiden, The Netherlands) prepared in the same buffer and left to equilibrate for 20 min at room temperature. Excitation was at 370 nm, and emission was recorded between 400 and 700 nm using 1.50-nm band-pass excitation and emission slits. Measurements were performed at 20 °C. The fluorescence signal obtained from the buffer alone with 20 μM ANS was subtracted. Measurements were confirmed with samples incubated for longer periods of time (2–3 h) at room temperature or at physiological salt concentrations (phosphate-buffered saline).

NMR Spectroscopy and Analysis—All ^1H-^{15}N heteronuclear single quantum coherence (HSQC) spectra were recorded on a Varian INOVA spectrometer at 600 MHz in 20 mM δ^3-sodium acetate (pH 4.0) (90% H_2O and 10% D_2O) at 25 °C. Sample concentrations were 0.6 mM (CCP1) and 0.7 mM (CCP12 and CCP2). The spectral widths were 5000 Hz in the ^1H dimension and 2000 Hz in the ^{15}N dimension for all spectra. The CCP1 spectrum was recorded with 64 scans and 512 increments in the ^{15}N dimension; the CCP2 spectrum was recorded with 8 scans and 128 increments in the ^{15}N dimension; and the CCP12 spectrum was recorded with 16 scans and 96 increments in the ^{15}N dimension. After processing, data matrices were 1024 points in ^1H and

256 points in ^{15}N. For each spectrum, a sine-bell square window function (with a shift of 90°) was applied in both dimensions.

Unlabeled, ^{15}N-labeled, and $^{13}C/^{15}N$-labeled CCP2 samples at a concentration of ~1 mM were prepared in 20 mM δ^3-sodium acetate (pH 4.0) (90% H_2O and 10% D_2O). Spectra were collected at 600 MHz (37 °C) except where stated. For resonance assignments, ^1H-^{15}N HSQC (34, 35) and ^1H-^{13}C HSQC (36) spectra were used along with the following three-dimensional heteronuclear experiments: CBCA(CO)NH and HNCACB (37), HBHA(CO)NH (38), HBHANH (39), (H)C(CO)NH-total correlation spectroscopy (TOCSY) and H(C)(CO)NH-TOCSY (40), HCCH-TOCSY (41), and (HB)CB(CGCD)HD and (HB)CB(CGCDCE)HE (42). 15N- and 13C- (at 800 MHz) edited NOESY experiments were collected with mixing times of 146 and 100 ms, respectively.

Hydrogen bond donors were identified from relatively slowly exchanging (>20 min) amides in a series of H_2O/D_2O exchange ^1H-^{15}N HSQC spectra, and proton acceptors were inferred from supporting nuclear Overhauser effect (NOE) data. A semiconstant time heteronuclear multiple/single quantum coherence was used to derive $J_{HNH\alpha}$ values (44). NMR data were processed within AZARA (available at www.bio.cam.ac.uk/azara) making use of maximal entropy methods to process the indirectly detected dimensions in three-dimensional experiments; spectra were viewed and assigned within ANSIG (45).

For ^{15}N T_1 measurements, delays of 6.75, 12.2, 328.3, 655.3, and 873.3 ms were used; for of ^{15}N T_2 measurements, delays of 17.02, 33.02, 65.02, 145.02, 161.02, and 177.02 ms were used (46). For each residue, a single exponential decay was fitted to the extracted peak heights, and relaxation times were calculated by nonlinear fitting. ^1H-^{15}N NOEs were calculated from the ratio of the intensities of the cross-peaks in the reference spectrum to those recorded in the spectrum in which the ^1H signals were saturated (47).

Structure Calculation and Comparisons—A second backbone ^{15}N-^1HN resonance was observed for each of 27 residues in the ^1H-^{15}N HSQC spectrum of CCP2, most of which were found in the region spanning Val^{111} to Phe^{128}. This second set of resonances was assigned to a minor form of CCP2, in which Pro^{119} is in the *cis*-conformation. Resolved ^{15}N- and ^{13}C-edited NOESY cross-peaks for both species were picked and assigned unambiguously whenever possible. A ratio of *trans*- to *cis*-conformer populations of 3:2 was estimated from ^1H-^{15}N HSQC cross-peak intensities, and this was used to scale the intensities of conformer-specific cross-peaks (48). The intensity of each such cross-peak was multiplied by the inverse of the proportion of the appropriate conformer (*i.e.* 5/3 for the *trans*-conformer and 5/2 for the *cis*-conformer). This compensates for the ratio of the populations of the two conformers present in the sample when converting NOEs to distance restraints.

The Connect program within AZARA was used to convert appropriately scaled cross-peak intensities into four distance categories with upper bounds of 2.7, 3.3, 5, and 6 Å. Unambiguous and ambiguous NOE restraint lists were generated with 0.05 and 0.3 ppm margins of error in the ^1H and $^{13}C/^{15}N$ dimensions, respectively. These restraint files along with the hydrogen bond restraints and $J_{HNH\alpha}$ values were input into a crystallography and NMR system-based structure calculation (49) using a simulated annealing protocol (50). Three (for the *trans*-conformer) and two (for the *cis*-conformer) "filtering" steps were performed on the ambiguous NOE list to remove assignment possibilities that contributed <1% to the total NOE intensity. Redundant NOE restraints were discarded, and structures were selected on the basis of having the lowest NOE-derived energies, no violations of distance restraints >0.5 Å, and no violations of coupling constants >1 Hz.

Combinatorial extension (51) was used to compare all 25 solved CCP modules individually against the *cis*- and *trans*-forms of the $GABA_B$ R1a CCP2 module. Multiprot (52) was used to calculate the multiple structure superposition of all solved CCP modules (including both $GABA_B$ R1a CCP2 forms).

RESULTS

Expression and Purification—P. pastoris is an appropriate organism for expression of CCP modules because it possesses the ability to promote disulfide bond formation and glycosylation (53, 54). In this study, *P. pastoris* was used to express the putative CCP modules of $GABA_B$ R1a as a module pair (CCP12) and as single modules (CCP1 and CCP2). All three protein fragments were secreted at useful levels (8–10 mg of protein/liter of BMGM) when the recombinant organisms were grown in shaking flasks. Lower induction temperature (25 °C instead of 30 °C as generally used for culturing *P. pastoris*), low pH (pH 3), and cycles of daily harvests, followed by cell resuspension in fresh induction medium, helped to maximize yield. (Note that samples from *P. pastoris* cultured at pH 3 were identical from a biophysical standpoint to protein produced by growth at pH 6 (data not shown).)

All fragments were purified by cation exchange chromatography, followed by reverse-phase chromatography. Note that alternative methods of purification, not incorporating a reverse-phase step, produced proteins with identical spectra (data not shown). Consensus *N*-glycosylation sites occur at Asn^{23} and Asn^{83}; and in this work, CCP1 and CCP12 were treated with endoglycosidase H_f. Following purification, each product showed one band upon SDS-PAGE (Fig. 1). Their identities were confirmed by N-terminal sequencing, which showed the presence of EF (from the DNA cloning strategy) or EAEF (the EA is left over from cleavage of the yeast α-factor signal sequence by Ste13) prior to the native sequence.

Mass Spectrometry—Electrospray ionization mass spectrometry of the $GABA_B$ CCP modules expressed in *P. pastoris* confirmed that their molecular masses match those expected if all cysteines are involved in disulphide formation (see "Supplemental Results"). In addition to a major species bearing one residual GlcNAc unit, minor components with no or two residual GlcNAc units were observed for CCP1 and CCP12. Oxidation of Met^{89} was also observed in most but not all CCP1 and CCP12 preparations and had no significant effect as judged by NMR spectroscopy. Trypsin digestion and quadrupole time-of-flight mass spectrometry confirmed the expected CCP module pattern of disulfide formation in CCP1.

Binding Experiments—Preliminary experiments carried out using the yeast two-hybrid system with a human brain cDNA library as prey and DNA fragments encoding the CCP modules of human $GABA_B$ receptors as bait indicated that CCP1 interacts with the C-terminal domain of fibulin-2. To confirm that the $GABA_B$ receptor CCP modules interact with fibulin-2, Trx-F2C was immobilized on Sepharose and used to affinity isolate the receptor from solubilized rat synaptic plasma membranes. The results shown in Fig. 2*b* indicate that both $GABA_B$ R1a and $GABA_B$ R1b were isolated from the solubilized synaptic membranes, but that the $GABA_B$ R1a subunit was substantially enriched in the isolate compared with the $GABA_B$ R1b subunit. To determine which of the $GABA_B$ R1 isoforms interacts with F2C, a similar affinity isolation was performed using lysates of cells permanently expressing the GABAB R1a or $GABA_B$ R1b subunit plus the $GABA_B$ R2 subunit. The $GABA_B$ R1a subunit was selectively isolated by incubation with the Trx-F2C fusion protein, whereas the $GABA_B$ R1b subunit appeared to be nonspecifically isolated under these conditions (Fig. 2*c*, *Con lanes*). In the case of the $GABA_B$ R1a subunit, both fully and non-glycosylated forms of the receptor were isolated, whereas with the $GABA_B$ R1b subunit, only the non-glycosylated intracellular pool of the protein was pulled down in both the specific and nonspecific incubations. There appeared to be a larger intracellular pool of the unglycosylated $GABA_B$ R1b subunit in the cell lysates (Fig. 2*c*, *Lys lanes*, compare the lower bands), and some of this material could be poorly folded and consequently give rise to nonspecific interactions with the affinity supports. Consistently, however, the $GABA_B$ R1a subunit was pulled down specifically in these experiments, suggesting that one or both of the CCP modules are important for the interaction with fibulin-2.

To confirm that the $GABA_B$ R1a CCP modules, as expressed in *P. pastoris*, retain the ability of the native receptor to bind fibulin-2, CCP12 was immobilized on Sepharose and then incubated with medium from cells secreting fibulin-2. Under

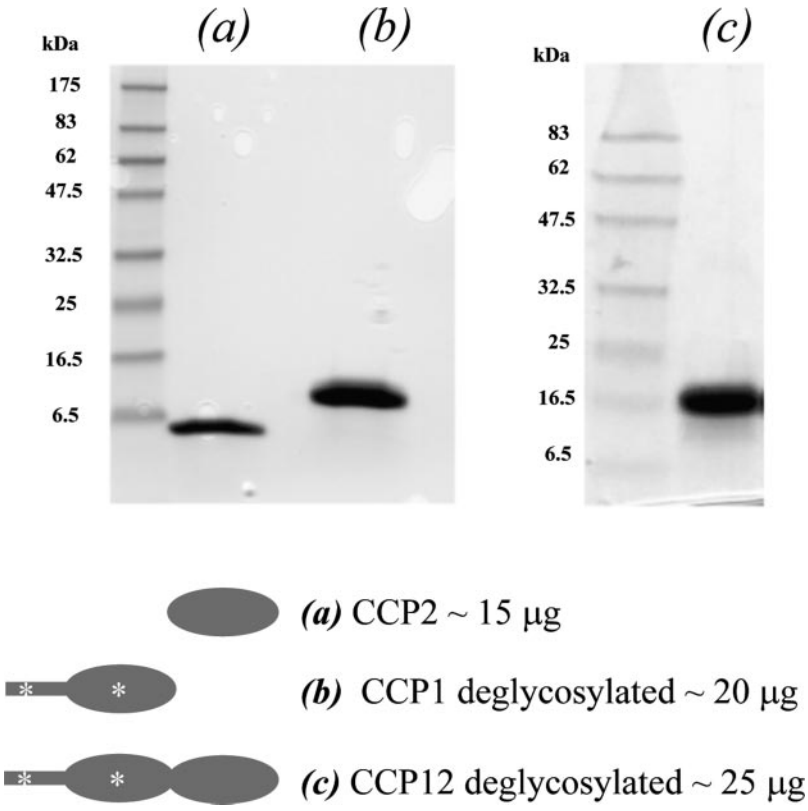

FIG. 1. **SDS-PAGE analysis of purified $GABA_B$ R1a CCP fragments.** $GABA_B$ R1a CCP fragments were separated by SDS-10–20% PAGE under reducing conditions and visualized using Coomassie Blue. The schematics depict the nature and quantity of the protein fragment in each lane. CCP modules are represented by *ellipses*, and *N*-glycosylation sites are indicated with *asterisks*. The non-consensus extension of seven residues at the beginning of CCP1 is indicated by a *thick line*.

these conditions, it was clear that fibulin-2 was indeed enriched in the eluates from immobilized CCP12-Sepharose, but not in those from control GST-Sepharose (Fig. 2*d*, *upper panel*). In all of these experiments, even when the C-terminally degraded form of fibulin-2 was present, the only form that was isolated by CCP12-Sepharose was full-length fibulin-2. This suggests that the C-terminal domain of fibulin-2 is necessary for the interaction. To determine which of the two CCP modules interacts with fibulin-2, the individual modules were immobilized on Sepharose. As shown in Fig. 2*d* (*lower panel*), CCP1 (but not CCP2) pulled down full-length fibulin-2. Thus, by affinity isolation of the native or recombinantly expressed $GABA_B$ R1a-$GABA_B$ R2 heterodimer with fibulin-2 and by isolation of fibulin-2 with the CCP modules expressed in *P. pastoris*, we have confirmed results based on yeast two-hybrid studies showing that these modules can interact with fibulin-2.

NMR Spectroscopy—The double module fragment (CCP12) was investigated by NMR spectroscopy prior to expression of the individual modules. Its ^{1}H-^{15}N HSQC spectrum contains an appropriate number of cross-peaks (Fig. 3*a*), but a proportion of these have relatively low intensity. Furthermore, a lack of transfer in TOCSY-type experiments was apparent (data not shown). Conformational heterogeneity was inferred from inspection of the region of the ^{1}H-^{15}N HSQC spectrum where three tryptophan NH$^{\epsilon 1}$ cross-peaks would be expected (~125–130 ppm ^{15}N and ~10–10.5 ppm ^{1}H). This inference was subsequently confirmed by analysis of individual modules (Fig. 3, *b* and *c*).

The ^{1}H-^{15}N HSQC spectrum of CCP1 is characterized by a mixture of sharp and broad resonances. Many of these signals have poor ^{1}H dispersion, implying that there is a substantial part of CCP1 that is not compactly structured. On the other hand, the presence of a number of dispersed non-glycine resonances in its ^{1}H-^{15}N HSQC spectrum indicates some structure within CCP1. The number of CCP1 cross-peaks and their dispersion in ^{1}H-^{15}N HSQC experiments showed no improvement over a wide range of pH values and under other conditions (including near-physiological conditions); pH 4 was chosen for most of the spectra to reduce solvent exchange of HN resonances. Neither the glycosylation state of CCP1, nor the absence (in the truncated version) of the N-terminal extension of seven residues (Gly^{17}–Asn^{23}) prior to the first consensus Cys, resulted in any significant improvement in the quality of the NMR spectra. The three-dimensional ^{15}N-edited NOESY spectra of CCP1 showed similarly poor overall dispersion, whereas even cross-peaks that are dispersed in the ^{1}H-^{15}N HSQC spectra showed few inter-residue NOEs. Only a small number of NOEs in the NH-NH region were present, and no NOEs could be observed between the high field-shifted methyl groups and HN resonances.

In contrast to the ^{1}H-^{15}N HSQC spectrum of CCP1, the CCP2 spectrum is characteristic of a well folded protein domain. The presence of some doubled cross-peaks is a consequence of *cis*/*trans*-isomerization of an *X*–Pro bond (see below). Standard sets of NMR experiments were collected on a ^{13}C/^{15}N-labeled sample of CCP2, analyzed, and used as a basis for three-dimensional structure calculations (below).

When ^{1}H-^{15}N HSQC spectra (Fig. 3, *d* and *e*) and three-dimensional ^{15}N-edited NOESY spectra (data not shown) recorded on CCP1, CCP2, and CCP12 were overlaid, they showed that the spectra of the module pair are simply additions, with only subtle differences, of the individual module spectra. For example, in regions where tryptophan, glycine, and serine/threonine peaks occur often (~108–113 ppm ^{15}N and ~8.3–8.7 ppm ^{1}H), most of the resolved spin systems observed in the CCP1 spectra are clearly identifiable in the CCP12 fragment, with no significant change in NOE patterns or chemical shifts. Likewise, most cross-peaks attributable to CCP2 are present in the CCP12 spectra. Few amide protons could be detected in the ^{1}H-^{15}N HSQC spectrum of CCP12 1 h after redissolving freeze-dried material in D_2O at 25 °C (data not shown). All of these were attributable to CCP2 and none to CCP1. Glycosylation of CCP12 did not significantly affect spectral quality (data not shown).

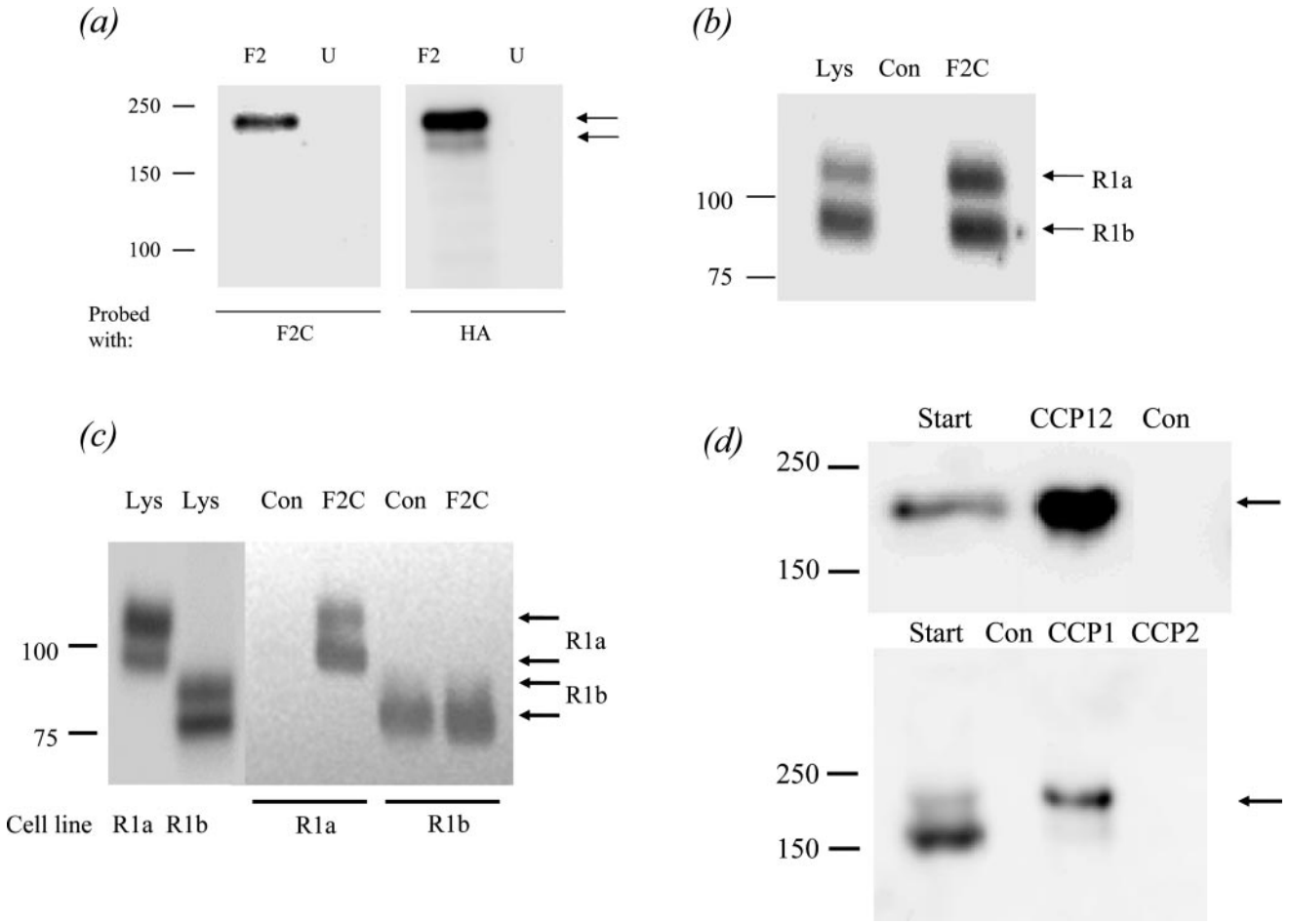

FIG. 2. **Interaction between fibulin-2 and GABA$_B$ R1a CCP modules.** *a*, characterization of HA-tagged fibulin-2 secreted from CHO cells permanently expressing the fibulin. Medium from the cells (*F2 lanes*) or from untreated normal CHO cells (*U lanes*) was analyzed on a 6% SDS-polyacrylamide gel and immunoblotted using either the anti-F2C Ab (raised against the C-terminal region of fibulin-2) or the anti-HA Ab. Both antibodies reacted with a band at >200 kDa, but the anti-HA Ab also showed a band at 180 kDa, which probably represents a C-terminally degraded form of fibulin. *b*, affinity isolation of rat synaptic GABA$_B$ receptors with the fibulin-2 interaction domain. Rat synaptic plasma membranes were solubilized with 1% (w/v) sodium deoxycholate, and the lysates were diluted 1:5 with 1% (v/v) Triton X-100 as described under "Experimental Procedures." The lysates (*Lys lane*) were incubated with either Trx-F2C-Sepharose (*F2C lane*) or control GST-Sepharose (*Con lane*), and the bound proteins were analyzed on a 7.5% SDS-polyacrylamide gel and probed for the presence of GABA$_B$ R1 using an antibody that reacts with both the GABA$_B$ R1a and GABA$_B$ R1b subunits. Similar results were obtained in five different experiments. *c*, affinity isolation of CHO cell-expressed GABA$_B$ receptors with the fibulin-2 interaction domain. CHO cells expressing either GABA$_B$ R1a or GABA$_B$ R1b with GABA$_B$ R2 were lysed in 1% (v/v) Triton X-100 as described under "Experimental Procedures." Lysates (*Lys lanes*) were incubated with either Trx-F2C-Sepharose (*F2C lanes*) or control GST-Sepharose (*Con lanes*), and the bound proteins were analyzed on a 7.5% SDS-polyacrylamide gel and probed for the presence of GABA$_B$ R1. Similar results were obtained in three separate experiments. *d*, *upper panel*, affinity isolation of fibulin-2 with CCP12-Sepharose. The CHO supernatant containing fibulin-2 (*Start lane*) was incubated with CCP12-Sepharose (*CCP12 lane*) or control GST-Sepharose (*Con lane*), and the bound proteins were subsequently eluted and analyzed on a 6% SDS-polyacrylamide gel and probed for the presence of HA-tagged fibulin. Similar results were obtained in three separate experiments. *Lower panel*, only CCP1-Sepharose (*CCP1 lane*) allows affinity isolation of full-length fibulin-2. The positions of Bio-Rad Precision-Plus prestained protein molecular mass markers are indicated in kilodaltons.

Differential Scanning Calorimetry—The thermal unfolding of the GABA$_B$ fragments was studied to probe their thermodynamic stability and tertiary structure. The DSC data for CCP12 and CCP2 (Fig. 4*a*) are consistent with a single endothermic transition in each case, with very similar midpoints (64.72 ± 0.03 and 66.59 ± 0.04 °C). In both cases, there was a nearly perfect agreement between calorimetric and van't Hoff enthalpies, which indicates that unfolding can be adequately approximated by a two-state mechanism and that no intermediates are present at equilibrium. No sign of visible precipitation was observed after the recordings. In contrast, the CCP1 DSC profile (Fig. 4*b*) has no heat absorption peak over the temperature range employed (22–100 °C), although a weak negative transition can be observed at ~52 °C prior to a substantial decline in heat capacity above 60 °C. The latter is probably due to the irreversible exothermic aggregation of the protein, but no evidence of precipitation was seen after the recordings. This result strongly suggests that recombinant CCP1 has little rigid tertiary structure, in contrast to CCP2. Moreover, the similarity of the calorimetric profiles obtained for CCP2 and CCP12 points to CCP1 having a lack of stable tertiary structure in the context of the module pair.

Circular Dichroism Spectroscopy—To complement NMR and DSC studies, far- and near-UV CD spectra were recorded on individual modules. Far-UV CD spectra of proteins are used to estimate their secondary structure content, whereas near-UV CD spectra are sensitive to the environments of aromatic side chains and have contributions from disulfide bonds. It has been previously reported that the far-UV CD spectra of compactly folded CCP modules are characterized by an unusual positive ellipticity in the 220–240 nm region (55); furthermore, it has

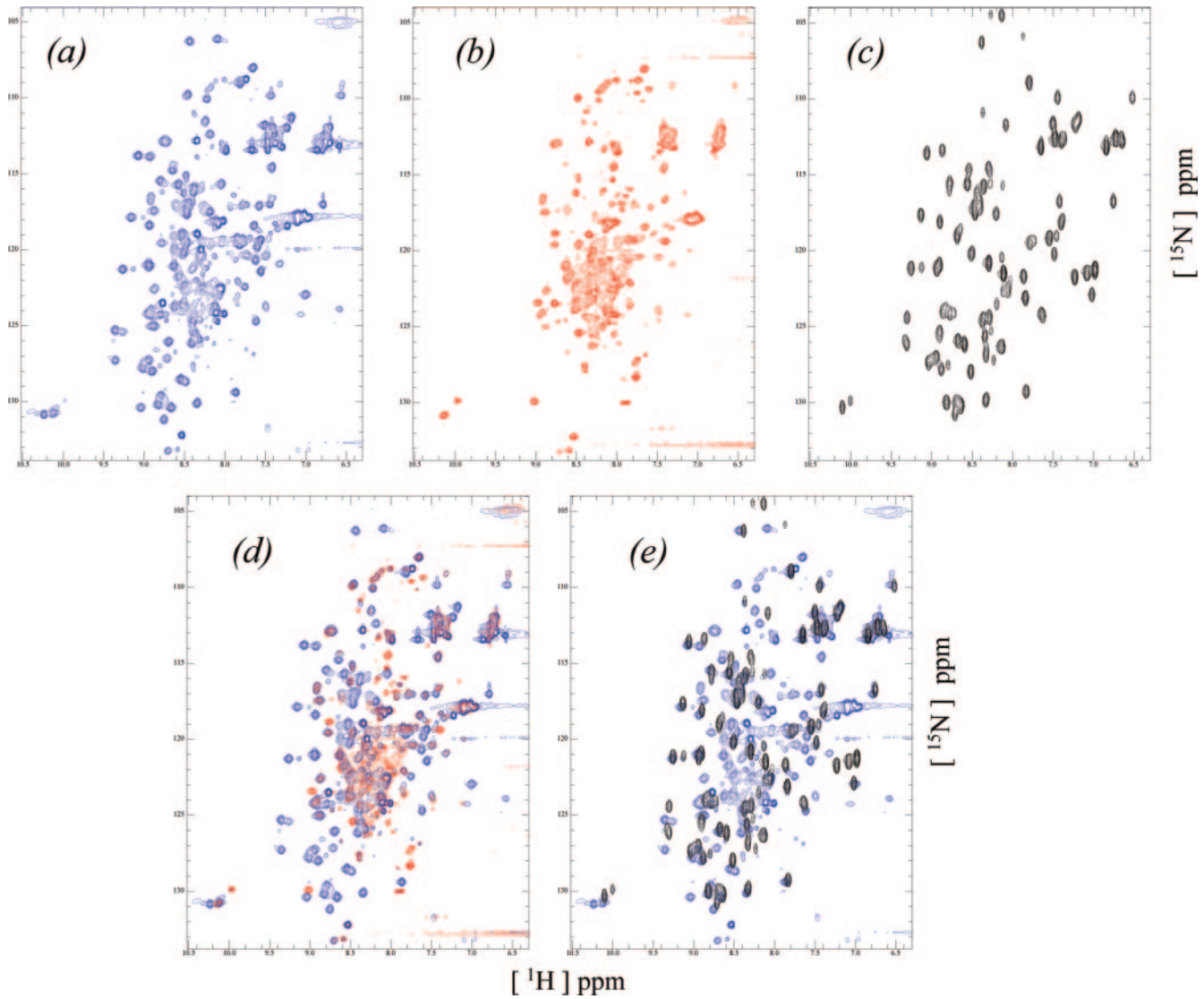

FIG. 3. **^{1}H-^{15}N HSQC spectra of GABA$_B$ R1a CCP modules.** *a*, ^{1}H-^{15}N HSQC spectrum of CCP12. *b*, ^{1}H-^{15}N HSQC spectrum of CCP1. *c*, ^{1}H-^{15}N HSQC spectrum of GABA$_B$ R1a CCP2. *d*, overlay of the ^{1}H-^{15}N HSQC spectra of CCP1 (*red*) and CCP12 (*blue*). *e*, overlay of the ^{1}H-^{15}N HSQC spectra of CCP2 (*black*) and CCP12 (*blue*).

been suggested that this characteristic could arise from the presence of tryptophan residues in β-strands (55). The near-UV CD spectra of CCP modules are dominated by a large negative band centered at 280 nm (55).

CCP1 showed a well defined positive ellipticity in the far-UV region centered at 228 nm (Fig. 5*a*), which was noteworthy in view of the low extent of folding implied by NMR spectroscopy and the lack of thermal stability inferred from the DSC studies. Moreover, CCP1 has a negative band centered at 280 nm (Fig. 5*b*). A positive ellipticity in the far-UV region (centered at 237 nm) and a very large negative band centered at 280 nm in the near-UV region were observed for CCP2 (Fig. 5, *c* and *d*), consistent with its compactly folded nature as determined by NMR and DSC.

CCP modules have two disulfide bonds and a conserved tryptophan that is found within the hydrophobic core of the module, close to the Cys-I–Cys-III disulfide bond. It is therefore possible that the negative ellipticity at 280 nm has contributions from disulfide bonds as well as contributions from aromatic amino acid side chains packed within the core. Either possibility is consistent with the effects of 10 mM DTT, which abolished the negative ellipticity in CCP1 (Fig. 5*b*). On the other hand, in the case of CCP2, 10 mM DTT diminished the 280 nm signal, but 20 mM DTT was required to abolish it completely (Fig. 5*d*). This result suggests that the CCP1 disulfide bonds are more accessible to DTT compared with CCP2. Whether the loss of signal in these cases is due to thermal melting of the hydrophobic cores or arises directly from reduction of the disulfide linkages (or a combination of the two) remains unknown.

Upon reduction with 10 mM DTT, the CCP1 far-UV positive ellipticity was abolished to a degree equivalent to that of the denatured (6 M GdnHCl) protein (Fig. 5*a*). On the other hand, CCP2 retained almost all its far-UV positive ellipticity at 20 mM DTT (Fig. 5*d*). Disulfide bond contributions to CD spectra are normally seen in the near-UV region, but they can also contribute to the intensity at ~225 nm, depending on their dihedral angle (56). The fact that 20 mM DTT (which, based on the evidence of the near-UV spectra, caused reduction of the disulfides in both CCP1 and CCP2) did not abolish the ellipticity of CCP2 at 237 nm implies that, in this case, the signal does not arise from the disulfides. Furthermore, this result indicates that a significant degree of secondary structure remains, even in the absence of disulfide bonds. On the other hand, in the case

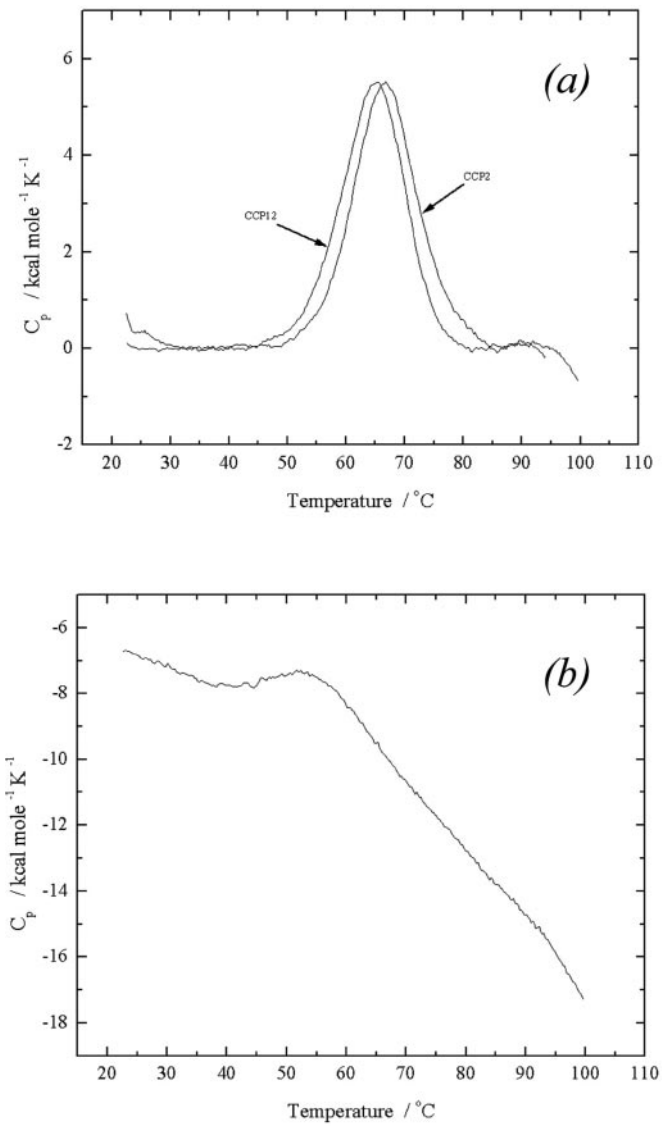

FIG. 4. **DSC studies on GABA$_B$ R1a CCP modules.** *a*, overlay of CCP12 and CCP2 DSC profiles; *b*, CCP1 DSC profile. Shown are concentration-normalized heat capacity (C_p) data with the control base line subtracted.

of CCP1, no detectable secondary structure remains once the disulfides are reduced.

The relative stability of each module was further investigated by recording far-UV CD spectra as a function of GdnHCl (Fig. 6*a*). CCP1 showed an almost complete loss of signal above 3.5 M GdnHCl, with a midpoint value of 1.8 M GdnHCl. This is a notably low value for a CCP module and implies that the secondary structural elements that give rise to this negative ellipticity are only marginally stable. By contrast, CCP2 showed little loss of secondary structure below 3 M GdnHCl and a total loss only at 7 M GdnHCl, with a midpoint value of between 5 and 5.5 M GdnHCl. CCP2 is therefore a particularly stable example of a CCP module, with a midpoint value higher than any of the previously reported CCP unfolding transitions. For example, the 16th CCP module of complement receptor type 1 has a midpoint of 4–4.5 M GdnHCl (55).

ANS Fluorescence Experiments—A well established and sensitive test to probe partial folding in globular proteins is the binding of the fluorophore ANS. Binding of a protein to ANS induces an increase in the fluorescence of ANS at 470 nm upon excitation at 370 nm. ANS binds to solvent-accessible hydrophobic regions in proteins. Although ANS has been shown to bind to surface-exposed patches of non-polar groups in compactly folded proteins, binding to a partially folded state is much stronger in general compared with the native or fully denatured state (57). ANS was found to bind only weakly to CCP2 (Fig. 6*b*). This weak binding is attributable to the presence of a hydrophobic patch seen in the NMR-derived structure (see Fig. 9). By contrast, ANS bound strongly to CCP1 (Fig. 6*b*). This is evidence of the presence of a substantial number of solvent-accessible non-polar groups in CCP1 and implies strongly that CCP1 is not compactly folded.

The double module (CCP12) at the same concentrations as CCP1 and CCP2 in the experiments described above exhibited a substantially higher degree of ANS binding compared with CCP2 alone. This is consistent with the failure of CCP2 to induce a compactly folded conformation of CCP1 in the double module. On the other hand, ANS binding was lower than that observed for CCP1 alone. This suggests that there is some degree of stabilization of CCP1 in the presence of CCP2.

Three-dimensional Structure of CCP2—Two ensembles each of 24 three-dimensional structures were calculated on the basis of experimental data: for a major form of CCP2 with the *trans*-configuration at the Leu^{118}–Pro^{119} peptide bond and for a similar (backbone root mean square deviation (r.m.s.d.) = 1.26 Å over all 61 residues) minor form with the *cis*-configuration at the Leu^{118}–Pro^{119} bond (Fig. 7, *a* and *b*). Structures representing the *trans*-form converge slightly better (Table I), reflecting the greater number of inter-residue NOEs available for the calculation. Taken together, the number of experimental restraints (an average of 10 unique and unambiguous inter-residue NOEs/residue in the *trans*-form), the low number of violations exhibited by the final structures, the good convergence, and the Ramachandran plot (>91% of residues in the most "favored" or "additional allowed" regions) indicate that a relatively good quality three-dimensional structure has been obtained for *trans*-CCP2. This is the first atomic resolution structural data for any part of the GABA$_B$ receptor. The *cis*- and *trans*-forms of the structure differ significantly only in the vicinity of the *cis*/*trans*-peptide bond (Fig. 7*c*). Because the *cis*-form is less populated in the NMR sample, the description below concentrates on the *trans*-form.

CCP2 has a three-dimensional structure (Fig. 7*c*) that resembles that of other CCP modules (24). Extended segments of polypeptide, some regions of which may be classified as β-strands, are connected by loops and turns. The extended segments run antiparallel to each other and form five staves of a barrel-like structure with N and C termini at opposite ends. Up to eight stretches of β-strand (strands A–H) occur in CCP modules (58), but in the case of *trans*-CCP2, only strands B and D–H (accounting for 23 residues in total) feature consistently among the 24 members of the ensemble of NMR-derived CCP2 structures. Residues corresponding to strands A and C do not satisfy the criteria of Kabsch and Sander (59) for β-strands in most cases. With six residues, strand D is the longest β-strand and forms part of a four-stranded antiparallel β-sheet with strands B and F (on either side of strand D) and strand G (on the other side of strand F); strands E and H form a separate, small two-stranded antiparallel β-sheet.

As in several other known examples of CCP modules, within the fourth stave of the barrel, a looped out section occurs between strands E and F (Fig. 7*c*). In most CCP modules, there is a region of high sequence and structural variation in the second stave, after strand B, termed the hypervariable loop or region (24). This frequently forms a lateral projection and has often been suggested as a likely interaction site. In CCP2, the hypervariable region does not project laterally; instead, it and

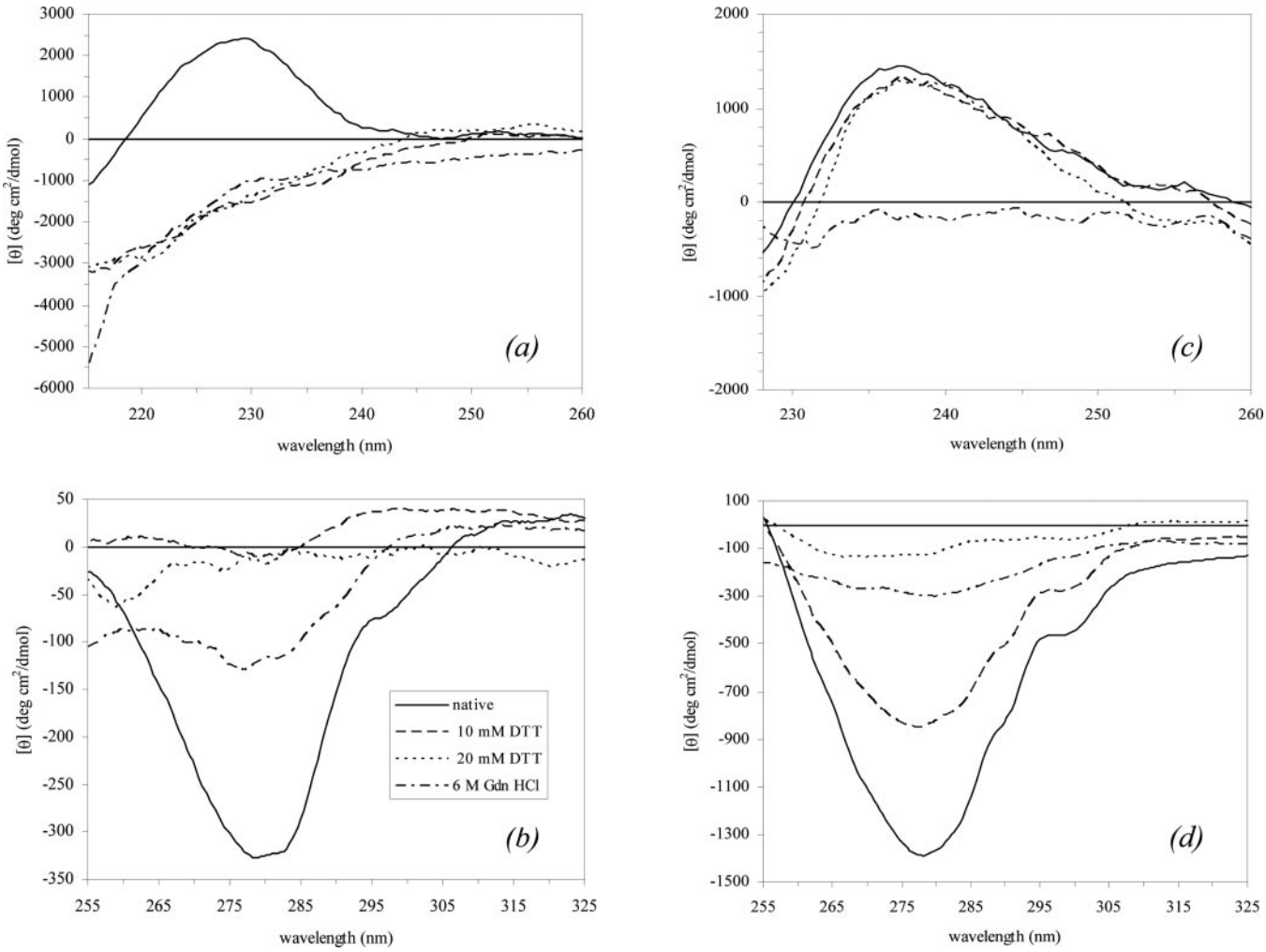

FIG. 5. **CD spectra of GABA$_B$ R1a CCP modules.** *a* and *b*, far- and near-UV CD spectra for CCP1, respectively; *c* and *d*, far- and near-UV for CCP2, respectively. CD spectra were collected under near physiological conditions (*solid lines*) and after incubation with 10 mM DTT (*dashed lines*), 20 mM DTT (*dotted lines*), or 6 M GdnHCl (*dashed and dotted lines*). *deg*, degrees.

the region corresponding to strand C in the classical CCP module structure form a prominent longitudinal projection. Among the family of 25 solved structures of CCP modules, this projection is unique. The sequence here is LPAL (where the Leu^{118}–Pro^{119} peptide bond is the source of the *cis*- and *trans*-forms of CCP2). In the *trans*-form, there is little evidence that this loop undergoes mobility on the nanosecond-to-picosecond time scale since heteronuclear NOEs in this region are not noticeably lower than average (Fig. 8*a*). On the other hand, in the minor *cis*-form, residues 117 and 118 do have lowered ^{1}H-^{15}N NOEs consistent with mobility on this rapid time scale. In both forms, several residues in the loop have shorter T_2 values and elevated T_1/T_2 ratios, suggestive of motion on the millisecond-to-microsecond time scale (Fig. 8, *b* and *c*). This hypervariable loop lies close to the N terminus of the CCP2 module, and therefore, in the intact receptor, it might be expected to interact with CCP1 and may have different dynamic properties.

In terms of overall structure, *trans*-CCP2 is most similar (Fig. 7*d*) to the third module of DAF (r.m.s.d. = 1.49 Å over 52 residues), the second CCP module of β_2-glycoprotein I (r.m.s.d. = 1.57 Å over 57 residues), and the first module of complement receptor type 2 (r.m.s.d. = 1.60 Å over 53 residues). It is least similar to the fifth module of factor H (r.m.s.d. = 3.86 Å over 57 residues). A very unusual feature of the CCP2 sequence is the lack of proline residues in the stretch following the first of the consensus cysteines. This is unique among CCP modules with solved three-dimensional structures, and the average number of proline residues here is two. This segment of CCP2 has a helical appearance (a short helical turn appears in 37.5% of the structure ensemble, including the closest-to-mean structure, with hydrogen bonds from the Ser^{100} oxygen to Tyr^{103} HN, the Lys^{101} oxygen to Leu^{104} HN, and the Ser^{102} oxygen to Thr^{105} HN), but nonetheless traces a similar overall path to the equivalent segments of conventional CCP modules. Compared with the third module of DAF, the second CCP module of β_2-glycoprotein I, and the first module of complement receptor type 2, CCP2 has a longer hypervariable region, which is accommodated in the unique longitudinal projection described above. Compared with the third module of DAF, CCP2 lacks an insertion in the EF loop. Both of these features are near the N terminus. Thus, when CCP2 is overlaid with its closest structural relative, the third module of DAF (Fig. 7*e*), the two structures are seen to be very similar indeed at their C-terminal ends, but diverge at their N-terminal ends.

CCP2 does not possess any outstanding electrostatic features (Fig. 9*a*) apart from a negatively charged patch close to its C terminus. The same face of CCP2 also carries several exposed hydrophobic side chains, including Phe^{112} and Leu^{113}, which are non-conserved (Fig. 9*b*), whereas the opposite face lacks any notable lipophilic characteristics.

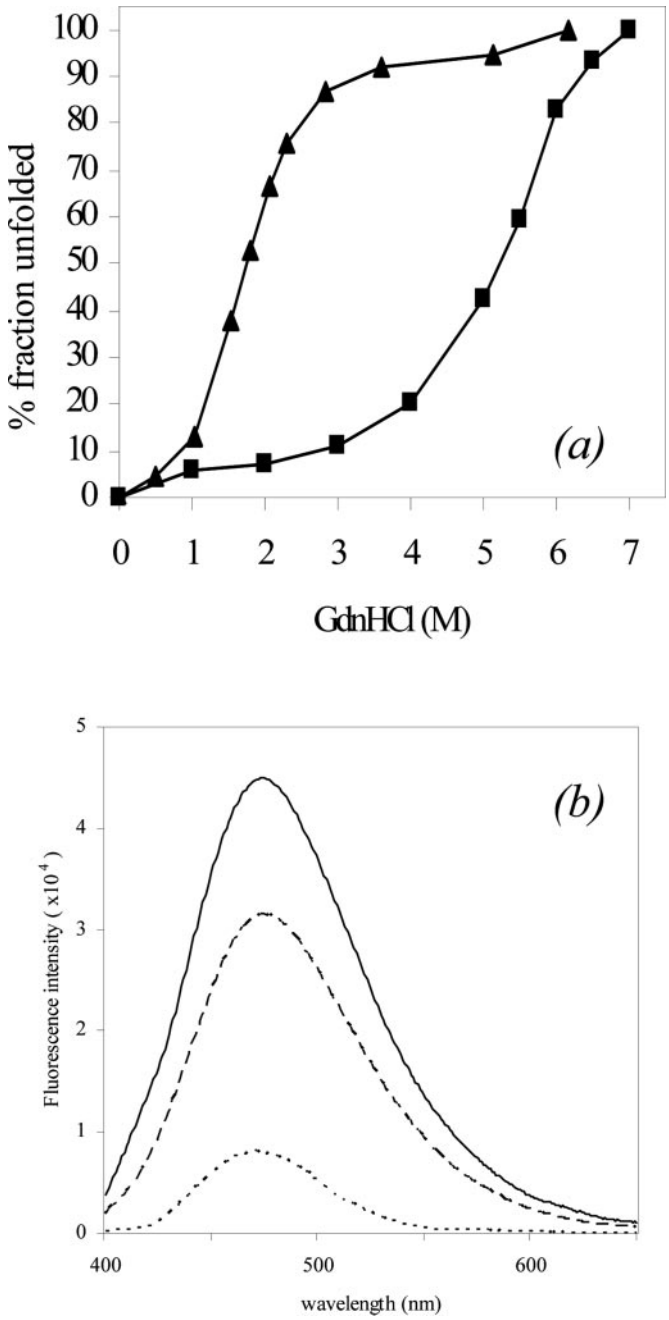

FIG. 6. **Structural integrity of CCP1 and CCP2.** *a*, denaturation. Protein fragments were incubated in increasing GdnHCl concentrations, and CD spectra were recorded. The observed change in ellipticity at 228 nm (CCP1) or 237 nm (CCP2) compared with the native protein at each concentration is expressed as a percentage of the total change in ellipticity induced by 6 M (CCP1; ▲) or 7 M (CCP2; ■) GdnHCl. *b*, fluorescence emission of ANS. CCP1 (*solid line*), CCP12 (*dashed line*), and CCP2 (*dotted line*) fragments (3.6 μM) were incubated for 20 min with ANS (20 μM) in 20 mM sodium phosphate (pH 7.5) at 20 °C. Excitation was at 370 nm, and emission was measured between 400 and 700 nm.

DISCUSSION

Preparation of CCP Modules from GABA$_B$ R1a—The work represents an additional example of the successful use of *P. pastoris* to express CCP modules in useful yields. Daily harvesting was required because CCP1 and CCP12 are susceptible to rapid cleavage (after Lys[51]) (data not shown). The presence of oxidized methionine was previously reported in recombinant CCP modules from complement receptor type 1 (60) and, as in the present case, had no significant effect upon three-dimensional structure. The variable levels of *N*-glycosylation at Asn[83] were anticipated from previous studies (22), but the presence or absence of glycosylation had no effect on the structure as judged by NMR or its stability according to DSC (data not shown). Asn[23] (in the seven-residue N-terminal extension; not present in the previously reported construct) was found to be *N*-glycosylated in this study. The presence or absence of this extension (with or without its glycan) had no significant effect upon structure or stability (data not shown). Nonetheless, large glycans are undesirable in NMR studies, so the carbohydrates were trimmed with endoglycosidase H_f to leave single GlcNAc residues. The high yield of protein expression and the formation of disulfides in the expected Cys-I–Cys-III and Cys-II–Cys-IV pattern are both consistent with proper processing by the secretory pathway. In previous studies (50), other CCP modules (*e.g.* from complement receptor type 1) were mutated to remove *N*-glycosylation sites prior to successful expression and structure determination. The possibility that the addition to the core sugars of more complex, branched saccharides (lacking in *P. pastoris*) is a specific structural requirement in CCP1 seems very unlikely.

Recombinant CCP Fragments from the GABA$_B$ Receptor Are Able to Bind to Fibulin-2—A useful criterion of the authenticity of a recombinant protein is its functional activity. Based on a preliminary yeast two-hybrid study, the putative CCP modules of the $GABA_B$ R1a subunit were reported to interact with the extracellular matrix protein fibulin-2 (17–20). In this study, this interaction was shown using pull down-type assays for the first time, thus confirming an intriguing interaction between the $GABA_B$ receptor and an extracellular matrix protein. That the CCP12 fragment expressed in *P. pastoris* could be used in affinity purification of fibulin-2 is also highly significant because this confirms that the material expressed in yeast retains one of the functional properties of the intact receptor. The previously reported yeast two-hybrid experiments were negative for CCP2 binding to fibulin-2 (18, 19). The results presented here confirm that CCP1, in both the native and recombinant forms, makes the major contribution to the interaction with fibulin-2.

The functional relevance of CCP1 interaction with fibulin-2 is still unknown. Fibulins are present in the central nervous system and are known to have roles in development (61). The $GABA_B$ R1a (two CCP modules) and $GABA_B$ R1c (possessing only CCP1) isoforms are more highly expressed in fetal brain compared with $GABA_B$ R1b (13), and this suggests a possible role for the interaction between CCP and fibulin-2 in human brain development. An interaction of the $GABA_B$ receptor (although not involving the CCP modules) with another extracellular matrix protein, tenascin-R, has also been reported (21). Tenascin-R was shown to modify $GABA_B$ receptor activity. Efforts to detect modulation of $GABA_B$ receptor activity by fibulin-2 are under way.

Unlike CCP2, CCP1 Is Not Compactly Folded—CCP1 and CCP2 are both expressed as soluble proteins in good yield, have appropriately paired disulfides, and yield similar far-UV CD profiles. On the other hand, they have contrasting biophysical properties. CCP2, which has a sequence more typical of CCP modules, is compactly folded. It is stable even at relatively high temperature or denaturant concentration, and its disulfide bridges and hydrophobic side chains are largely buried and generally not accessible to solvent (only a small level of ANS binding was detected), giving rise to a very strong near-UV negative ellipticity. Its three-dimensional structure was solved, yielding the first structural information for any part of the $GABA_B$ receptor. The structure of CCP2 is similar to the struc-

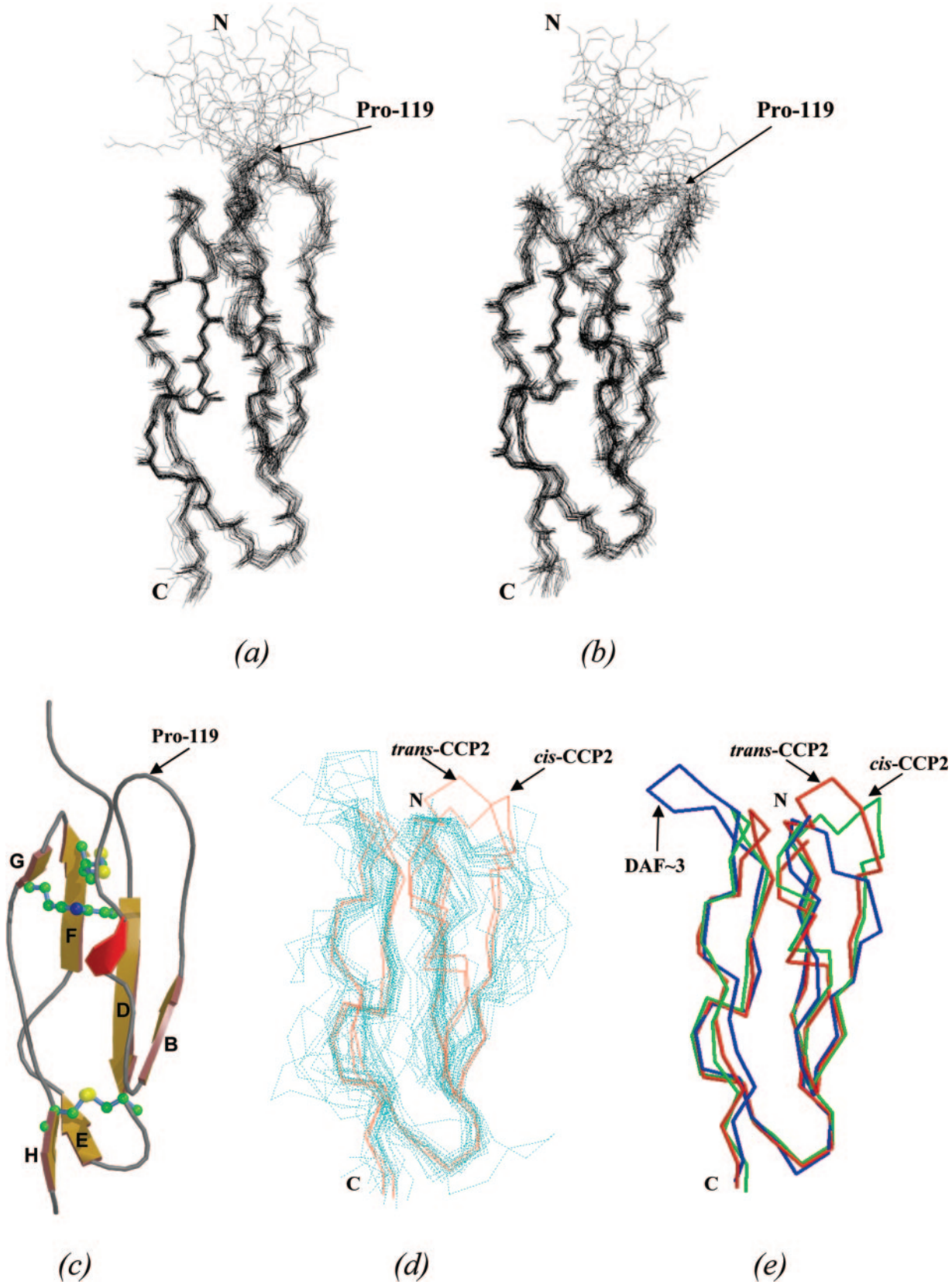

FIG. 7. **Solution structure of $GABA_B$ R1a CCP2.** A total of 24 structures are shown as backbone traces overlaid on all C-α atoms from Cys^{99} to Cys^{156}. *a*, structures of the *trans*-form. *b*, structures of the *cis*-form. See Table I for r.m.s.d. *c*, Molscript (71) representation of the closest-to-mean structure of the *trans*-form. Assignment of β-strands was based on a consensus among members of the ensemble (Procheck-NMR (72)) and annotated according to Henderson *et al.* (58). Cysteines and tryptophan are shown in ball-and-stick representation. *d*, C-α trace superposition (52) of all solved CCP module structures (*trans*-CCP2 and *cis*-CCP2 in *red* and 25 others in *cyan*). *e*, view of *trans*-CCP2 (*red*) and *cis*-CCP2 (*green*) superimposed (all equivalent C-α atoms (52)) on the structure they resemble most closely, that of the third module of DAF (*DAF~3*; *blue*) using Multiprot. Images in *d* and *e* were produced using RasMol (73).

TABLE I
Structural statistics for $GABA_B$ R1a CCP2

	trans	*cis*
Restraints used for structure calculation		
Total unambiguous NOEs[a]	1363	1268
Total ambiguous NOEs	100	79
Total	1463	1347
For unambiguous NOEs		
Intraresidue ($i \rightarrow i$)	636	632
Sequential ($i \rightarrow i + 1$)	303	273
Short-range ($i \rightarrow i + (2–4)$)	85	75
Long-range ($i \rightarrow i + (>4)$)	339	288
J coupling (HN → HA)	20	23
Hydrogen bonds	11	11
r.m.s.d. from experimental restraints		
NOEs (Å)	0.021 ± 0.0016	0.020 ± 0.0018
J restraints	0.99 ± 0.09°	0.98 ± 0.08°
r.m.s.d.from idealized geometry		
Bond lengths (Å)	0.00164 ± 0.00011	0.00163 ± 0.000095
Bond angles	0.331 ± 0.0157°	0.330 ± 0.0159°
Dihedrals	16.34 ± 0.54°	16.06 ± 0.46°
ϕ *vs.* ψ (%)		
Residues in most favored regions	67.3	70.2
Residues in additional allowed regions	24.4	22.4
Residues in generously allowed regions	5.2	5.1
Residues in disallowed regions	3.1	2.4
Coordinate r.m.s.d. (Å) from average module structure		
Backbone atoms C-α, N, CO (99–159)[b]	0.60	0.73
C-α only (99–159)[b]	0.62	0.76
All heavy atoms (99–159)[b]	1.38	1.46

[a] All statistics are for 24 structures from 120 calculated. 975 restraints were the same for both structure calculations.
[b] Where residues that have heteronuclear NOE values <1 S.D. lower than the mean are excluded from the r.m.s.d. calculation.

tures of CCP modules in complement regulators except for the region near the N terminus. The hypervariable loop of CCP2 extends toward the N terminus and may participate in the junction with CCP1.

In contrast, CCP1 has marginal stability. It exposes many of its hydrophobic side chains to solvent (as inferred from ANS binding), implying a poorly structured hydrophobic core, albeit one that generates a weak near-UV ellipticity. The results from a range of biophysical methods are all consistent with the poor quality of NMR spectra, which precluded any attempts at backbone assignment. Taken together, the biophysical data suggest that CCP1 contains a mixture of ordered and molten globular parts. The presence of the ordered parts would explain the limited number of proteolytically sensitive sites observed in the mass spectrometric investigations and explains the cooperative unfolding of CCP1 with increasing GdnHCl concentrations as monitored by far-UV CD. That no such cooperative transition was seen by DSC may reflect aggregation competing with the unfolding event during the heating process. The presence of partially ordered structure is also consistent with ANS binding.

Although it could be argued that the poorly structured nature of CCP1 is an artifact of expression, the compact folding of CCP2 and the successful expression in *P. pastoris* of many other CCP modules suggest otherwise (50, 58, 62–64). Furthermore, when the two modules are expressed together, the second (but not the first) module is compactly folded, and there is only a small degree of stabilization imparted to CCP1 by CCP2 despite the potential for a relatively extensive intermodular junction involving the hypervariable loop of CCP2. Most important, the recombinant material is "functional" in the sense that it is able to bind to an extracellular matrix protein. The possibility that CCP1 has different biophysical properties in the context of the intact receptor (perhaps through intrasubunit contacts or through contacts with the $GABA_B$ R2 subunit) cannot of course be ruled out.

Disorder Is Important for Function?—Numerous examples of functionally competent proteins with a high content of native disorder exist intracellularly, and several extracellular examples are now recognized (65, 66). The common occurrence of native disorder has been recognized in the availability of the software tool PONDR (Predictor of Natural Disordered Regions) (67–69). The CCP1 and CCP2 sequences were submitted to PONDR. The region from Arg^{67} to Val^{77} of CCP1 was predicted as disordered. This corresponds (according to a multiple sequence alignment (22)) to strands E and F in CCP modules of known structure. PONDR did not predict disorder in CCP2, and no or very little disorder was predicted in the CCP modules of *Vaccinia* virus complement control protein and membrane cofactor protein. Disorder might also be expected in the region of CCP1 corresponding to the hypervariable loop in other CCP modules, which is uncommonly long. In this respect, it is interesting to note that Lys^{51}, where CCP1 proteolytic cleavage occurs, is predicted to be part of the hypervariable loop. However, in the absence of a backbone assignment, it is difficult to infer from the experimental data the precise extent of disorder in CCP1.

Despite the relative lack of precedent for a disulfide-stabilized extracellular protein domain with a high degree of native disorder, we do know from studies of dynamics in other examples that CCP modules are relatively flexible on a range of time scales. For example, in no CCP module studied so far are there any amide protons that persist for more than a few hours after dissolving a protonated CCP module in D_2O. Furthermore, some CCP modules display a wide range of ^1H-^{15}N NOEs and backbone ^{15}N order parameters throughout their sequence, indicative of motion on a fast time scale. They also contain a high proportion of residues undergoing slow (millisecond-to-microsecond) conformational rearrangements. Another N-terminal CCP module (the first CCP module of membrane cofactor protein) with several binding partners was found to have more mobility than an internal module (the 16th CCP module of complement receptor type 1) (70). Therefore, it is conceivable that a spectrum of mobilities exists among CCP modules and that CCP1 of the $GABA_B$ receptor lies at one extreme. Proteins with high levels of native disorder are thought of in terms of the advantage such conformational plasticity affords in terms of

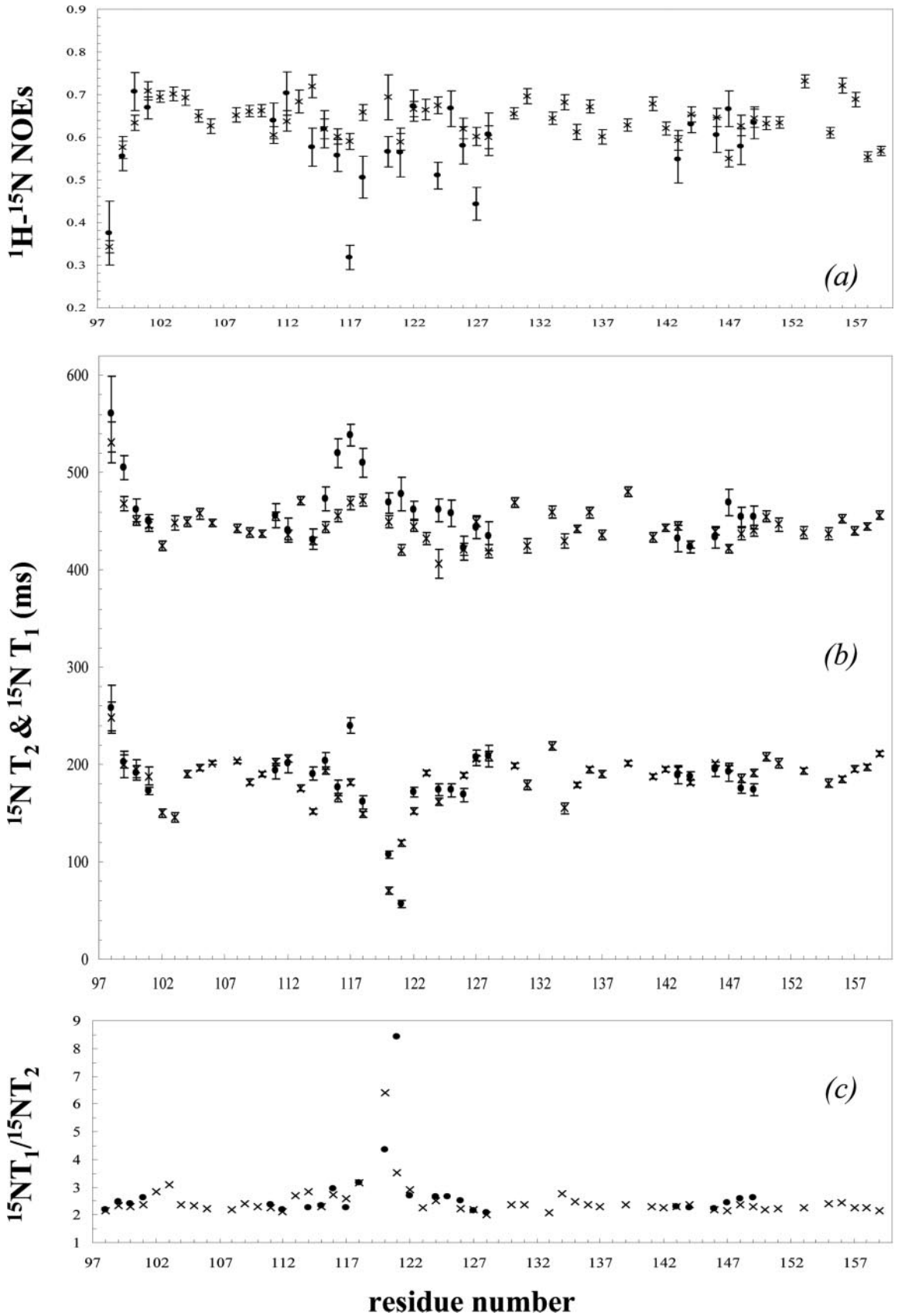

FIG. 8. **NMR relaxation data for GABA$_B$ R1a CCP2.** *a*, heteronuclear NOEs for *trans*-CCP2 (×) and *cis*-CCP2 (●); *b*, ^{15}N T_2 (*upper*) and ^{15}N T_1 (*lower*) values for *trans*-CCP2 (×) and *cis*-CCP2 (●); *c*, ^{15}N T_1/^{15}N T_2 ratio for *trans*-CCP2 (×) and *cis*-CCP2 (●).

displaying a range of affinities for a variety of ligands. In this respect, it is interesting to note that our yeast two-hybrid screens identified the C-terminal domain of all five members of the fibulin family. The exact purpose of the N-terminal CCP modules that differentiate GABA$_B$ R1a from GABA$_B$ R1b is unknown, but the results presented here suggest that they

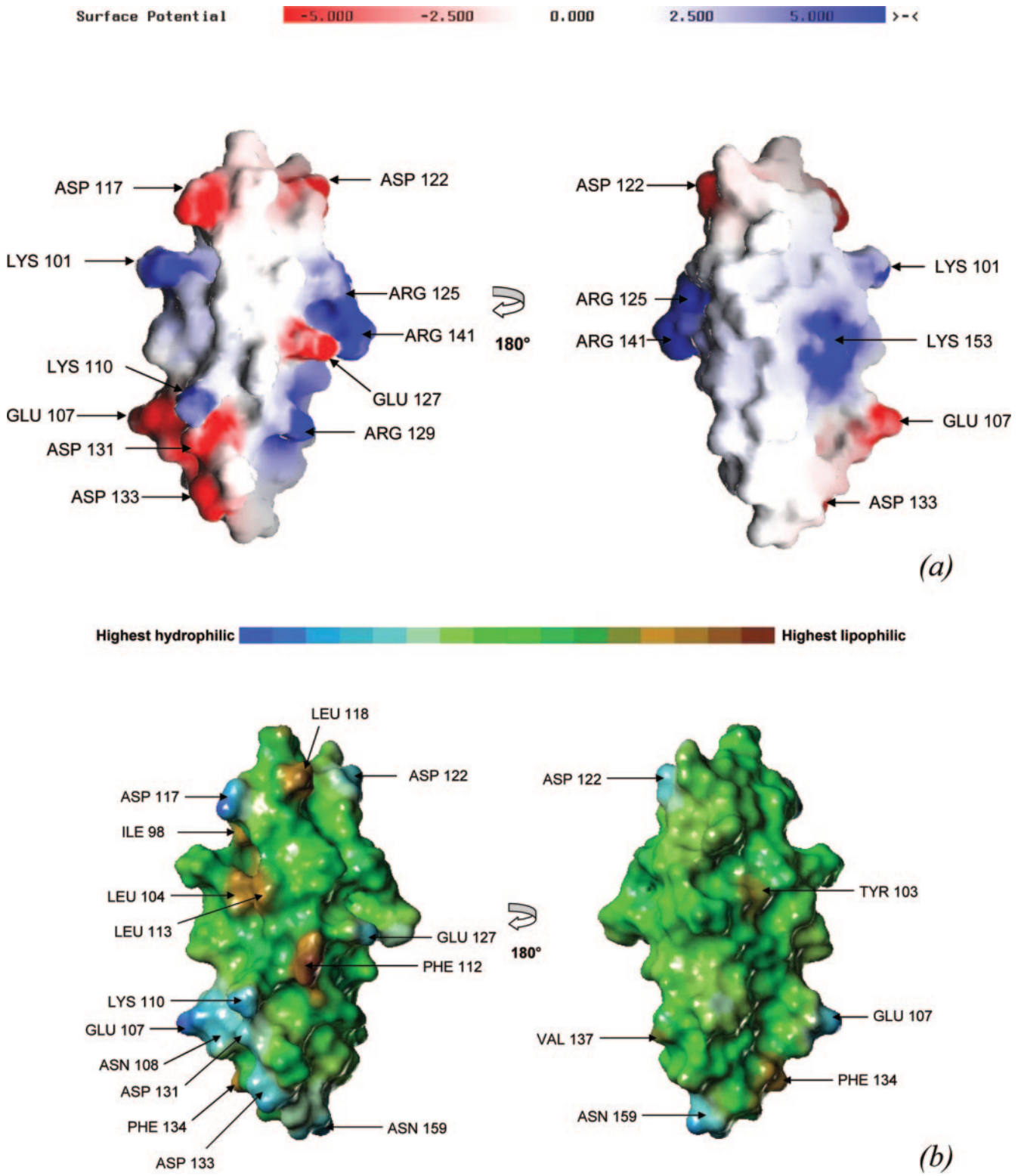

FIG. 9. **Surface features of GABA$_B$ R1a CCP2.** *a*, two side views rotated by 180° along the *y* axis depicting the GRASP (74) electrostatic surface rendition of *trans*-CCP2. Negatively charged (acidic) residues are colored *red*, and positively charged (basic) residues are colored *blue* (range of −5 to +5 kT where k = Boltzman's constant and T = temperature in Kelvins). *b*, lipophilic surface: two views rotated by 180° along the *y* axis depicting the MOLCAD (75) lipophilic surface rendition of *trans*-CCP2. The regions of high hydrophilicity are colored *blue*, and the regions of high lipophilicity (hydrophobicity) are colored *brown*.

could participate in protein-protein interactions with several extracellular matrix proteins.

Acknowledgements—We thank Prof. Alan Cooper and Margaret Nutley (University of Glasgow) for expert assistance with the calorimetry studies. We are also grateful to Prof. Lindsay Sawyer and Dr. Andreas Hofmann (University of Edinburgh) for help with recording and analyzing the CD and fluorescence data.

REFERENCES

1. Blein, S., Hawrot, E., and Barlow, P. (2000) *Cell. Mol. Life Sci.* **57,** 635–650
2. Bowery, N. G., Bettler, B., Froestl, W., Gallagher, J. P., Marshall, F., Raiteri,

M., Bonner, T. I., and Enna, S. J. (2002) *Pharmacol. Rev.* **54,** 247–264
3. Couve, A., Moss, S. J., and Pangalos, M. N. (2000) *Mol. Cell. Neurosci.* **16,** 296–312
4. White, J. H., Wise, A., Main, M. J., Green, A., Fraser, N. J., and Disney, G. H. (1998) *Nature* **396,** 679–682
5. Kaupmann, K., Malitschek, B., Schuler, V., Heid, J., Froestl, W., and Beck, P. (1998) *Nature* **396,** 683–687
6. Jones, K. A., Borowsky, B., Tamm, J. A., Craig, D. A., Durkin, M. M., and Dai, M. (1998) *Nature* **396,** 674–679
7. Kuner, R., Köhr, G., Grünewald, S., Eisenhardt, G., Bach, A., and Kornau, H. C. (1999) *Science* **283,** 74–77
8. Pin, J.-P., Galvez, T., and Prezeau, L. (2003) *Pharmacol. Ther.* **98,** 325–354
9. Robbins, M. J., Calver, A. R., Filippov, A. K., Hirst, W. D., Russell, R. B., Wood, M. D., Nasir, S., Couve, A., Brown, D. A., Moss, S. J., and Pangalos, M. N. (2001) *J. Neurosci.* **21,** 8043–8052
10. Duthey, B., Caudron, S., Perroy, J., Bettler, B., Fagni, L., Pin, J.-P., and Prezeau, L. (2002) *J. Biol. Chem.* **277,** 3236–3241
11. Galvez, T., Duthey, B., Kniazeff, J., Blahos, J., Rovelli, G., Bettler, B., Prezeau, L., and Pin, J.-P. (2001) *EMBO J.* **20,** 2152–2159
12. Liu, J., Maurel, D., Etzol, S., Brabet, I., Ansanay, H., Pin, J.-P., and Rondard, P. (2004) *J. Biol. Chem.* **279,** 15824–15830
13. Calver, A. R., Medhurst, A. D., Robbins, M. J., Charles, K. J., Evans, M. L., Harrison, D. C., Stammers, M., Hughes, S. A., Hervieu, G., Couve, A., Moss, S. J., Middlemiss, D. N., and Pangalos, M. N. (2000) *Neuroscience* **100,** 155–170
14. Martin, S. C., Russek, S. J., and Farb, D. H. (2001) *Gene* (*Amst.*) **278,** 63–79
15. Isomoto, S., Kaibara, M., Sakurai-Yamashita, Y., Nagayama, Y., Uezono, Y., and Yano, K. (1998) *Biochem. Biophys. Res. Commun.* **253,** 10–15
16. Schwarz, D. A., Barry, G., Eliasof, S. D., Petroski, R. E., Conlon, P. J., and Maki, R. A. (2000) *J. Biol. Chem.* **275,** 32174–32181
17. Calver, A. R., Davies, C. H., and Pangalos, M. (2002) *Neurosignals* **11,** 299–314
18. White, J. H., Ginham, R. L., Pontier, S., Wise, A., Blein, S., Barlow, P. N., Bouvier, M., and McIlhinney, R. A. J. (2002) *FENS Abstr.* **1,** 062.1
19. Ginham, R. L., Blein, S., Barlow, P. N., White, J. H., and McIlhinney, R. A. J. (2002) *FENS Abstr.* **1,** 144.6
20. Milligan, G., and White, J. H. (2001) *Trends Pharmacol. Sci.* **22,** 513–518
21. Saghatelyan, A. K., Snapyan, M., Gorissen, S., Meigel, I., Mosbacher, J., Kaupmann, K., Bettler, B., Kornilov, A. V., Nifantiev, N. E., and Sakanyan, V. (2003) *Mol. Cell. Neurosci.* **24,** 271–282
22. Hawrot, E., Xiao, Y., Shi, Q. L., Norman, D., Kirkitadze, M., and Barlow, P. N. (1998) *FEBS Lett.* **432,** 103–108
23. Bettler, B., Kaupmann, K., and N. G. Bowery, (1998) *Curr. Opin. Neurobiol.* **8,** 345–350
24. Kirkitadze, M. D., and Barlow, P. N. (2001) *Immunol. Rev.* **180,** 146–161
25. Herbst, R., and Nicklin, M. J. (1997) *Brain Res. Mol. Brain Res.* **44,** 309–322
26. Shimizu-Nishikawa, K., Kajiwara, K., and Sugaya, E. (1995) *Biochem. Biophys. Res. Commun.* **216,** 382–389
27. Imoto, T., and Yamada, H. (1997) in *Protein Function: A Practical Approach* (Creigthon, T. E., ed) pp. 279–316, IRL Press at Oxford University Press, Oxford
28. Rees, S., Coote, J., Stables, J., Goodson, S., Harris, S., and Lee, M. G. (1996) *BioTechniques* **20,** 102–110
29. Pan, T.-C., Sasaki, T., Lang, R. Z., Fassler, R., Timpl, R., and Chu, M. L. (1993) *J. Cell Biol.* **123,** 1269–1277
30. Molnar, E., McIlhinney, R. A. J., Baude, A., Nusser, Z., and Somogyi, P. (1994) *J. Neurochem.* **63,** 683–693
31. White, J. H., McIllhinney, R. A., Wise, A., Ciruela, F., Chan, W. Y., Emson, P. C., Billinton, A., and Marshall, F. H. (2000) *Proc. Natl. Acad. Sci. U. S. A.* **97,** 13967–13972
32. Pace, C. N., Shirley, B. A., and Thomson, J. A. (1990) in *Protein Structure: A Practical Approach* (Creigthon, T. E., ed) 2nd Ed., pp. 311–331, IRL Press at Oxford University Press, Oxford
33. Privalov, P. L., and Potekhin, S. A. (1986) *Methods Enzymol.* **131,** 4–51
34. Mori, S., Abeygunawardana, C., Johnson, M. O., and van Zijl, P. C. M. (1995) *J. Magn. Reson.* **108,** 94–98
35. Sklenar, V., Piotto, M., and Leppik, R. (1993) *J. Magn. Reson.* **102,** 241–245
36. Vuister, G. W., and Bax, A. (1992) *J. Magn. Reson.* **98,** 428–435
37. Muhandiram, D. R., and Kay, L. E. (1994) *J. Magn. Reson.* **103,** 203–216
38. Grzesiek, S., and Bax, A. (1993) *J. Biomol. NMR* **3,** 185–204
39. Wang, A. C., Lodi, P. J., and Qin, J. (1994) *J. Magn. Reson.* **105,** 196–198
40. Grzesiek, S., Anglister, J., and Bax, A. (1993) *J. Magn. Reson.* **101,** 114–119
41. Kay, L. E., Xu, G. Y., Singer, A. U., Muhandiram, D. R., and Forman-Kay, J. D. (1993) *J. Magn. Reson.* **101,** 333–337
42. Yamazaki, T., Forman-Kay, J. D., and Kay, L. E. (1993) *J. Am. Chem. Soc.* **115,** 11054–11055
43. Pascal, S. M., Muhandiram, D. R., Yamazaki, T., Forman-Kay, J. D., and Kay, L. E. (1994) *J. Magn. Reson.* **103,** 197–201
44. Aitio, H., and Permi, P. (2000) *J. Magn. Reson.* **143,** 391–396
45. Kraulis, P. J. (1989) *J. Magn. Reson.* **24,** 627–633
46. Kay, L. E., Nicholson, L. K., Delagio, F., Bax, A., and Torchia, D. A. (1992) *J. Magn. Reson.* **97,** 359–375
47. Grzesiek, S., and Bax, A. (1993) *J. Am. Chem. Soc.* **115,** 12593–12594
48. Yuan, X., Werner, J. M., Knott, V., Handford, P. A., Campbell, I. D., and Downing, K. (1998) *Protein Sci.* **7,** 2127–2135
49. Brunger, A. T., Adams, P. D., Clore, G. M., DeLano, W. L., Gros, P., Grosse-Kunstleve, R. W., Jiang, J. S., Kuszewski, J., Nilges, M., Pannu, N. S., Read, R. J., Rice, L. M., Simonson, T., and Warren, G. L. (1998) *Acta Crystallogr. D Biol. Crystallogr.* **54**, 905–921
50. Smith, B. O., Mallin, R., Krych-Goldberg, M., Wang, X., Hauhart, R. E., Bromek, K., Uhrin, D., Atkinson, J. P., and Barlow, P. N. (2002) *Cell* **108,** 769–780
51. Shindyalov, I., and Bourne, P. (1998) *Protein Eng.* **11,** 739–747
52. Shatsky, M., Nussinov, R., and Wolfson, H. J. (2002) *Proc. Lect. Notes Comput. Sci.* **2452,** 235–250
53. White, C. E., Kempi, N. M., and Komives, E. A. (1994) *Structure* **2,** 1003–1005
54. Cereghino, J. L., and Cregg, J. M. (2000) *FEMS Microbiol. Rev.* **24,** 45–66
55. Kirkitadze, M. D., Krych, M., Uhrin, D., Dryden, D. T., Smith, B. O., Cooper, A., Wang, X., Hauhart, R., Atkinson, J. P., and Barlow, P. N. (1999) *Biochemistry* **38,** 7019–7031
56. Kelly, S. M., and Price, N. C. (1997) *Biochim. Biophys. Acta* **1338,** 161–185
57. Kirkitadze, M. D., Barlow, P. N., Price, N. C., Kelly, S. M., Boutell, C. J., Rixon, F. J., and McClelland, D. A. (1998) *J. Virol.* **72,** 10066–10072
58. Henderson, C. E., Bromek, K., Mullin, N. P., Smith, B. O., Uhrin, D., and Barlow, P. N. (2001) *J. Mol. Biol.* **307,** 323–339
59. Kabsch, W., and Sander, C. (1983) *Biopolymers* **22,** 2577–2637
60. Mallin, R. L. (2003) *A Structural Study of the C3b-binding Site of Complement Receptor Type 1 (CD 35).* Ph.D. thesis, University of Edinburgh
61. Timpl, R., Sasaki, T., Kostka, G., and Chu, M. L. (2003) *Nat. Rev. Mol. Cell. Biol.* **4,** 479–489
62. Wiles, A. P., Shaw, G., Bright, J., Perczel, A., Campbell, I. D., and Barlow, P. N. (1997) *J. Mol. Biol.* **272,** 253–265
63. Murthy, K. H., Smith, S. A., Ganesh, V. K., Judge, K. W., Mullin, N., Barlow, P. N., Ogata, C. M., and Kotwal, G. J. (2001) *Cell* **104,** 301–311
64. Uhrinova, S., Lin, F., Ball, G., Bromek, K., Uhrin, D., Medof, M. E., and Barlow, P. N. (2003) *Proc. Natl. Acad. Sci. U. S. A.* **100,** 4718–4723
65. Dunker, A. K., Brown, C. J., Lawson, J. D., Iakoucheva, L. M., and Obradovic, Z. (2002) *Biochemistry* **41,** 6573–6582
66. Dunker, A. K., Lawson, J. D., Brown, C. J., Williams, R. M., Romero, P., Oh, J. S., Oldfield, C. J., Campen, A. M., Ratliff, C. M., Hipps, K. W., Ausio, J., Nissen, M. S., Reeves, R., Kang, C., Kissinger, C. R., Bailey, R. W., Griswold, M. D., Chiu, W., Garner, E. C., and Obradovic, Z. (2001) *J. Mol. Graph. Model.* **19,** 26–59
67. Romero, P., Obradovic, Z., Li, X., Garner, E., Brown, C., and Dunker, A. K. (2001) *Proteins* **42,** 38–48
68. Romero, P., Obradovic, Z., and Dunker, A. K. (1997) *Genome Inform. Ser. Workshop Genome Inform.* **8,** 110–124
69. Li, X., Romero, P., Rani, M., Dunker, A. K., and Obradovic, Z. (1999) *Genome Inform. Ser. Workshop Genome Inform.* **10,** 30–40
70. O'Leary, J. M., Bromek, K., Black, G. M., Uhrinova, S., Schmitz, C., Wang, X., Krych, M., Atkinson, J. P., Uhrin, D., and Barlow, P. N. (2004) *Protein Sci.* **13,** 1238–1250
71. Kraulis, P. J. (1991) *J. Appl. Crystallogr.* **24,** 946–950
72. Laskowski, R. A., Rullmann, J. A., MacArthur, M. W., Kaptein, R., and Thornton, J. M. (1996) *J. Biomol. NMR* **8,** 477–486
73. Sayle, R. A., and Milner-White, E. J. (1995) *Trends Biochem. Sci.* **20,** 374–376
74. Nicholls, A., Sharp, K. A., and Honig, B. (1991) *Proteins* **11,** 281–296
75. Heiden, W., Goetze, T., and Brickmann, J. (1993) *J. Comput. Chem.* **14,** 246–250